Estimates of Freshwater Discharge from Continents: Latitudinal and Seasonal Variations

AIGUO DAI AND KEVIN E. TRENBERTH

National Center for Atmospheric Research, Boulder, Colorado*

(Manuscript received 22 March 2002, in final form 12 July 2002)

ABSTRACT

Annual and monthly mean values of continental freshwater discharge into the oceans are estimated at 1° resolution using several methods. The most accurate estimate is based on streamflow data from the world's largest 921 rivers, supplemented with estimates of discharge from unmonitored areas based on the ratios of runoff and drainage area between the unmonitored and monitored regions. Simulations using a river transport model (RTM) forced by a runoff field were used to derive the river mouth outflow from the farthest downstream gauge records. Separate estimates are also made using RTM simulations forced by three different runoff fields: 1) based on observed streamflow and a water balance model, and from estimates of precipitation *P* minus evaporation *E* computed as residuals from the atmospheric moisture budget using atmospheric reanalyses from 2) the National Centers for Environmental Prediction–National Center for Atmospheric Research (NCEP–NCAR) and 3) the European Centre for Medium-Range Weather Forecasts (ECMWF). Compared with previous estimates, improvements are made in extending observed discharge downstream to the river mouth, in accounting for the unmonitored streamflow, in discharging runoff at correct locations, and in providing an annual cycle of continental discharge. The use of river mouth outflow increases the global continental discharge by ~19% compared with unadjusted streamflow from the farthest downstream stations. The river-based estimate of global continental discharge presented here is 37 288 ± 662 $km^3\ yr^{-1}$, which is ~7.6% of global *P* or 35% of terrestrial *P*. While this number is comparable to earlier estimates, its partitioning into individual oceans and its latitudinal distribution differ from earlier studies. The peak discharges into the Arctic, the Pacific, and global oceans occur in June, versus May for the Atlantic and August for the Indian Oceans. Snow accumulation and melt are shown to have large effects on the annual cycle of discharge into all ocean basins except for the Indian Ocean and the Mediterranean and Black Seas. The discharge and its latitudinal distribution implied by the observation-based runoff and the ECMWF reanalysis-based *P*–*E* agree well with the river-based estimates, whereas the discharge implied by the NCEP–NCAR reanalysis-based *P*–*E* has a negative bias.

1. Introduction

In a steady state, precipitation *P* exceeds evaporation *E* (or evapotranspiration) over land and the residual water runs off and results in a continental freshwater discharge into the oceans. Within the oceans, surface net freshwater fluxes into the atmosphere are balanced by this discharge from land along with transports within the oceans. The excess of *E* over *P* over the oceans results in atmospheric moisture that is transported onto land and precipitated out, thereby completing the land–ocean water cycle. While *E* and *P* vary spatially, the return of terrestrial runoff into the oceans is mostly concentrated at the mouths of the world's major rivers, thus providing significant freshwater inflow locally and thereby forcing the oceans regionally through changes in density (Carton 1991; Nakamura 1996).

To study the freshwater budgets within the oceans, therefore, estimates of continental freshwater discharge into the ocean basins at each latitude are needed. Baumgartner and Reichel (1975, BR75 hereafter) derived global maps of annual runoff and made estimates of annual freshwater discharge largely based on streamflow data from the early 1960s analyzed by Marcinek (1964). Despite various limitations of the BR75 discharge data (e.g., rather limited station coverage, areal integration over 5° latitude zones, no seasonal values), these estimates are still widely used in evaluations of ocean and climate models (Pardaens et al. 2002) and in estimating oceanic freshwater transport (Wijffels et al. 1992; Wijffels 2001), mainly because there have been few updated global estimates of continental discharge. The primary purpose of this study is to remedy this situation.

Correct simulations of the world river system and its routing of terrestrial runoff into the oceans has also become increasingly important in global climate system

* The National Center for Atmospheric Research is sponsored by the National Science Foundation.

Corresponding author address: A. Dai, National Center for Atmospheric Research, P.O. Box 3000, Boulder, CO 80307.
E-mail: adai@ucar.edu

models (Miller et al. 1994). For evaluating climate models, a few streamflow datasets have been compiled (e.g., Dümenil et al. 1993), although many studies included only 50 or so of the world's largest rivers. Other approaches (e.g., Hagemann and Gates 2001) utilize daily precipitation and parameterized evaporation to compute runoff that is then fed into a hydrological discharge model. This approach makes no use of actual measurements of discharge. Perry et al. (1996) gave an updated estimate of annual-mean river discharge into the oceans by compiling published, gauge-data-based estimates for 981 rivers. However, although they used the farthest downstream gauges, the distances to the river mouths ranged from 100 to 1250 km and they made no adjustments for this. They estimated the contributions from ungauged small rivers by fitting a power law to the dataset and extrapolating.

For years hydrologists have been improving terrestrial runoff fields. One such example is the work by Fekete et al. (2000, 2002), who used a global river discharge dataset from the Global Runoff Data Centre (GRDC) coupled with a simulated river network and a water balance model to derive a set of monthly global maps of runoff at 0.5° resolution. This merging approach offers the best estimate of the geography of terrestrial runoff, with the magnitude of runoff constrained by the observed discharge, while at the same time preserving the spatial distribution of the water balance. For oceanic water budget analyses, however, only the discharges at coastal river mouths are of interest. To estimate continental discharge using the runoff fields, a river transport model that routes the terrestrial runoff into the correct river mouths is needed. Alternatively, estimates can be made from gauge records of streamflow (e.g., Grabs et al. 1996, 2000), but then the issue of ungauged streams has to be addressed and extrapolation from the gauging station to the river mouth is needed. To our knowledge, neither of these approaches has been done thoroughly in estimating continental discharge, and much improved estimates are the main purpose of this study.

In a steady state, $P–E$ is a good proxy of runoff over land (BR75). Short-term $P–E$ may, however, differ from runoff because of changes in storage and, in particular, snow accumulation and melt and infiltration of water into the ground. On a day-to-day basis, runoff greatly depends upon the frequency, sequence, and intensity of precipitation and not just amount, as these factors alter the extent to which water can infiltrate and be stored in the soil. Changes in soil moisture can be important, and it is only on annual and longer timescales that conditions may approximate a steady state.

Another problem is human interference with the natural water flows. The mining of groundwater effectively changes the subterranean water storage, although it is offset to some extent by the filling of surface reservoirs. The biggest human influence comes from irrigation and water usage, although this should be reflected in the $P–E$ used in this study, which was derived from atmospheric moisture budget analyses. For the Mississippi River basin, for instance, Milly and Dunne (2001) estimate precipitation as 835 mm yr^{-1} and total evaporation as 649 mm yr^{-1}, of which consumptive use contributes 12 mm yr^{-1} (1.8%); surface reservoir filling provides a loss of 1 mm yr^{-1}; and groundwater mining adds 2 mm yr^{-1}. Overall, the changes in storage over land, such as in lakes and reservoirs, and through melting of glaciers are manifested as changes in sea level. Estimates of glacier contributions are 0.2 to 0.4 mm yr^{-1} and terrestrial storage -1.1 to 0.4 mm yr^{-1} (Church et al. 2001). Note that 1 mm yr^{-1} globally is equivalent to a volume of 357 km^3 yr^{-1} and is approximately the mean annual flow of the river Amur in Russia (Table 2). Nevertheless, these values are small compared with regional $P–E$ values.

Substantial problems still exist in analyzed fields of precipitation and evaporation based upon four-dimensional data assimilation (Trenberth and Guillemot 1996, 1998; Trenberth et al. 2001b; Maurer et al. 2000). In fact problems exist in all precipitation products (e.g., Yang et al. 2001; Adler et al. 2001; Nijssen et al. 2001), and evaporation is not measured but can only be estimated from bulk formulas. Potential evapotranspiration is measured from pans, but is not a measure of actual evaporation, and over the United States, estimated trends in actual evaporation and pan evaporation are opposite (Milly and Dunne 2001) because increased clouds reduce the latter, while increased soil moisture from increased precipitation (associated with the cloud increase) increases the availability of moisture for evaporation. Therefore, we believe that the $P–E$ used here, which was computed as a residual of the atmospheric moisture budget, is potentially much more promising.

Relatively new $P–E$ estimates were derived from the atmospheric moisture budget based on the National Centers for Environmental Prediction–National Center for Atmospheric Research (NCEP–NCAR, NCEP hereafter) reanalyses (Kalnay et al. 1996) by Trenberth and Guillemot (1996, 1998) and the European Centre for Medium-Range Weather Forecasts (ECMWF) ERA-15 reanalyses (Gibson et al. 1997) by Trenberth et al. (2001a). New $P–E$ estimates will also be produced for the ERA-40 reanalyses that are under way. One test for the $P–E$ fields is to compute the implied continental discharge and compare with that derived from gauge data. Unfortunately, the results using model-based P and E are not good (Oki 1999) because these are purely model-predicted fields. Although not problem free, $P–E$ estimates as a residual of the atmospheric moisture budget are better partly because atmospheric wind and moisture fields were calibrated every 6 h by atmospheric sounding and satellite observations in the reanalyses. They depend critically on atmospheric low-level divergence fields, which have considerable uncertainties, but small-scale errors naturally cancel as averages are taken over larger areas, and the global mean is guaranteed to balance. If the reanalysis data are evaluated to be re-

TABLE 1. Datasets used in this study. All are monthly.

Variables	Type and coverage	Resolution (°)	Period	Source and reference
Streamflow	Station, land		1–100+ yr	NCAR; Bodo (2001)
Runoff	Composite, land	0.5	Climatology	GRDC–UNH; Fekete et al. (2000)
E–P	NCEP–NCAR reanalysis, global	2.8	1979–95	NCAR; Trenberth and Guillemot (1998)
E–P	ECMWF reanalysis, global	2.8	1979–93	NCAR; Trenberth et al. (2001a)
P	Gauge plus satellite plus reanalysis, global	2.5	1979–98	CMAP; Xie and Arkin (1997)
P	Gauge plus satellite, global	2.5	1979–99	GPCP; Huffman et al. (1997)
T	Station data, land	0.5	1961–90	CRU; New et al. (1999)
River basin attributes	Simulated river network, STN-30p	0.5		UNH; Vörösmarty et al. (2000)

liable for estimating continental discharge, then they can be applied[1] to study the interannual to decadal variations of continental discharge because the reanalysis data are, or will be, available for the last 40–50 yr, and are likely to be updated regularly. This could become a valuable application of the reanalysis data given that many rivers have no or only short records of streamflow and that there has been a widespread decline in the number of river gauges during the last few decades (Shiklomanov et al. 2002).

In this study, we analyze station records of streamflow for 921 of the world's largest rivers to provide new estimates of long-term mean annual and monthly continental freshwater discharge into the oceans through each 1° latitude × 1° longitude coastal box. We make use of the composite runoff fields of Fekete et al. (2000, 2002), a state-of-the-art database of the world river network, and a river transport model (RTM) to translate information from the farthest downstream station to the river mouth, and to estimate contributions from unmonitored river basins. We also derive continental discharges using RTM simulations forced with various estimates of terrestrial runoff, including *P–E* from the reanalyses from NCEP–NCAR and ECMWF. Hence we compare the runoff-implied continental discharges with the gauge-based estimate.

Our goal is to update and improve the continental discharge estimates of BR75 and provide an evaluation of the *P–E* fields from the reanalyses, and at the same time provide useful data (e.g., river mouth flow rates) for climate model evaluations. The continental discharge can then be applied to produce detailed estimates of mean meridional freshwater transport by the oceans that can also be used in climate and ocean model evaluations.

2. Datasets

We used a number of observational and reanalysis data sets in this study, as listed in Table 1 and described below. The *P–E* data were remapped onto the 0.5° grid for driving the RTM.

Gauge records of streamflow rates are the basic data for estimating continental discharge. We used monthly streamflow datasets compiled by Bodo (2001) and others that are archived at NCAR (ds552.1, ds553.2, ds550.1; available online at http://dss.ucar.edu/catalogs/ranges/range550.html), together with the R-ArcticNET v2.0, a dataset created by C. J. Vörösmarty [University of New Hampshire (UNH)] et al. (online at http://www.R-ArcticNET.sr.unh.edu) that contains streamflow data for the Arctic drainage basins. These datasets were created using various sources of streamflow data, including those collected by the United Nations Educational Scientific and Cultural Organization (UNESCO), the United States Geological Survey (USGS), UNH, Russia's State Hydrological Institute, the GRDC in Germany (only an earlier version of its collection), and many national archives such as those for South American nations. Data quality controls were applied during the compilation, primarily for errata and inconsistencies in metadata. Undoubtedly, errors and discrepancies remain, although the majority of the streamflow records are thought to have an accuracy to within 10%–20% (Fekete et al. 2000).

After eliminating duplicate stations (mainly through locations), there were 8878 gauge records of monthly mean river flow rates with varying lengths, ranging from a few years to over 100 yr. The latest year with data is 2000, although most records end earlier (many in the 1990s). For estimating continental discharge, we selected 921 near-coastal (i.e., the farthest downstream) stations (Fig. 1) from this merged global streamflow dataset using a procedure described in section 3. Most of the selected stations are close to river mouths and have 10 or more years of data, although a few of them are located far from the ocean [e.g., Niger (~1000 km), Mekong (~850 km), Irrawaddy (~800 km)] or have only a few years of data that may not be representative of long-term means (cf. Table 2 and the appendix). The mean streamflow and drainage area data from these coastal stations were used to derive the river outflow into ocean at the river mouth, as described in section

[1] On annual and seasonal timescales, changes in soil moisture must be considred.

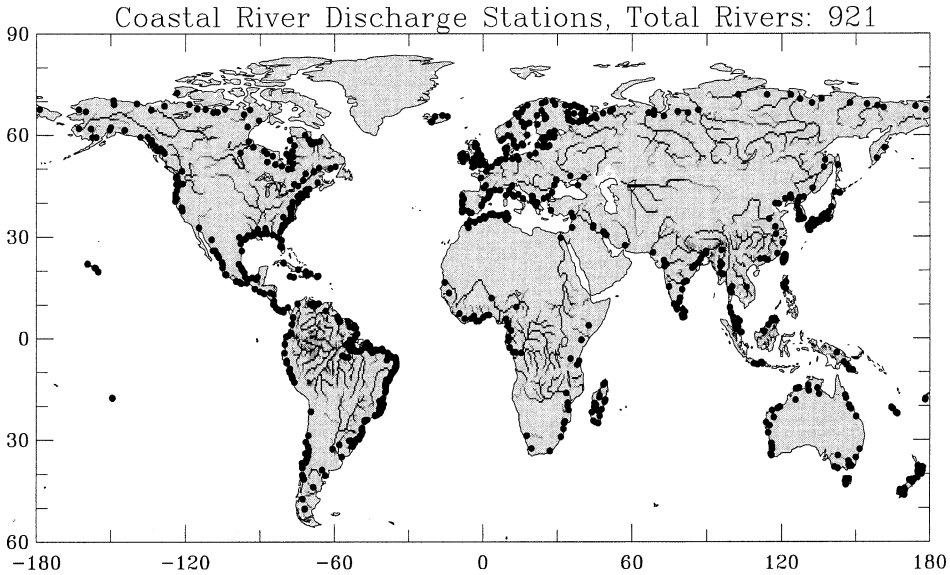

FIG. 1. Distribution of the farthest downstream stations for world largest 921 rivers included in this study. Also shown are the world major river systems simulated by a river transport model.

3. Because of the varying time periods of records, the mean river flow rates derived from these gauge records may be inconsistent temporally among the rivers.

To derive estimates of continental discharge independent of those based on the streamflow records and to estimate the discharge from the land areas that were not monitored by the gauges, we used the composite monthly and annual runoff fields of long-term means of Fekete et al. (2000, 2002). Although only 663 gauges were used and biases are likely over regions with little calibration, their composite fields at 0.5° resolution probably represent one of the best estimates of terrestrial runoff currently available.

We used the *P–E* fields derived from atmospheric moisture budget analyses based on the NCEP reanalyses for 1979–95 (Trenberth and Guillemot 1998) and ECMWF reanalyses for 1979–93 (Trenberth et al. 2001a). These data are available online from NCAR's Climate Analysis Section catalog (http://www.cgd.ucar.edu/cas/catalog/). We did not use the individual *E* and *P* fields from the reanalysis products.

We also used monthly and annual precipitation over land, derived by averaging the Climate Prediction Center Merged Analysis of Precipitation (CMAP) and the Global Precipitation Climatology Project (GPCP) climatology (Table 1). These products are based mainly on rain gauge measurements over land and, therefore, depend on the distribution of gauges. In many open areas this is adequate, but it is typically inadequate in mountainous areas, where gradients of precipitation are very large. Much more detailed estimates of precipitation by the Parameter-elevation Regressions on Independent Slopes Model (PRISM) at resolution of 2.5′ for the United States by Daly et al. (1994) have been compared with GPCP results by Nijssen et al. (2001), who found substantial discrepancies, usually underestimates of precipitation, over mountains in GPCP. Nevertheless, the CMAP- and GPCP-averaged precipitation was used to compute the river-basin-integrated precipitation and to help evaluate the *P–E* products.

For estimating snow effects on the annual cycle of runoff, we used a simple scheme that requires daily surface air temperature. The latter was interpolated from the New et al. (1999) monthly climatology.

To perform areal averaging and integration and to obtain estimates of drainage area for individual river basins, a database for the world river network is needed. We used the simulated river database STN-30p (Vörösmarty et al. 2000), a global simulated topological network at 30′ spatial resolution. The STN-30p contains 397 named large river basins and 5755 unnamed small river basins for the world river network. In this database, each 0.5° cell of land surface belongs to a river basin. The database includes, among others, the upstream drainage area for each cell and the exact location where the runoff generated in any given cell enters an ocean or sea.

3. Analysis procedure

a. Selection of coastal stations

Ignoring discharge of groundwater, the continental freshwater discharge is the sum of river outflows into the oceans. The farthest downstream gauging station (i.e., the station with the largest drainage area) for each river that reaches the ocean is the obvious choice for our purpose. Selecting the most-downstream stations for all the ocean-reaching rivers, while excluding upstream stations, from the 8878 stations in the merged stream-

TABLE 2. World's largest 50 rivers (by the estimated river mouth flow rate, Vol). Listed are long-term mean station (Stn, ± std dev) and river transport model (RTM) simulated river flow (in $km^3\ yr^{-1}$) at the station location, and the estimated annual volume (vol) and drainage area (DA, based on STN-30p, in $10^3\ km^2$) at the river mouth. The composite annual runoff data of Fekete et al. (2000) were used in the RTM simulation. Nyr is station record length in yr, lat and lon are latitude and longitude (negative in the Western Hemisphere) for the station.

		Vol at station		River mouth		Stn				
No.	Name	Str ± std dev	RTM	Vol	DA	DA	Nyr	Lon (°)	Lat (°)	Station, Country
1	Amazon	5330 ± 426	5083	6642	5854	4619	49	−55.5	−2.0	Obidos, Brazil
2	Congo	1271 ± 130	1266	1308	3699	3475	81	15.3	−4.3	Kinshasa, Congo
3	Orinoco	984 ± 112	1141	1129	1039	836	66	−63.6	8.1	Pte Angostu, Venezuela
4	Changjiang	910 ± 133	996	944	1794	1705	49	117.6	30.8	Datong, China
5	Brahmaputra	613 ± 51	617	628	583	555	6	89.7	25.2	Bahadurabad, Bangladesh
6	Mississippi	536 ± 130	458	610	3203	2896	71	−90.9	32.3	Vicksburg, MS, United States
7	Yenisey	577 ± 42	525	599	2582	2440	60	86.5	67.4	Igarka, Rusia
8	Paraná	476 ± 96	589	568	2661	2346	89	−60.7	−32.7	Timbues, Argentina
9	Lena	526 ± 63	456	531	2418	2430	60	127.4	70.7	Kusur, Russia
10	Mekong	292 ± 33	271	525	774	545	7	105.8	15.1	Pakse, Laos
11	Tocantins	356 ± 64	398	511	769	742	20	−49.7	−3.8	Tucurui, Brazil
12	Tapajos	337 ± 32	545	415	502	387	24	−56.8	−5.2	Jatoba, Brazil
13	Ob	397 ± 61	433	412	2570	2430	65	66.6	66.6	Salekhard, Russia
14	Ganges	382 ± 76	428	404	956	952	21	88.1	24.5	Farakka, India
15	Irrawaddy	258 ± 29	324	393	406	118	11	96.0	21.9	Sagaing, Myanmar (Burma)
16	St. Lawrence	226 ± 26	318	363	1267	774	64	−74.7	45.0	Cornwall, ON, Canada
17	Amur	312 ± 60	359	354	2903	1730	54	137.0	50.5	Komsomolsk, Russia
18	Xingu	272 ± 44	325	302	497	446	26	−52.2	−3.2	Altamira, Brazil
19	Mackenzie	288 ± 29	260	290	1713	1660	21	−133.7	67.5	Arctic Red, Canada
20	Xijiang	221 ± 45	179	270	409	330	46	111.3	23.5	Wuzhou, China
21	Columbia	172 ± 33	194	252	724	614	121	−121.2	45.6	The Dalles, OR, United States
22	Magdalena	231 ± 35	175	231	252	257	19	−74.9	10.2	Calamar, Colombia
23	Uruguay	165 ± 54	65	228	356	249	12	−58.0	−31.4	Concordia, Argentina
24	Yukon	203 ± 18	203	212	852	831	21	−162.9	61.9	Pilot Station, AK, United States
25	Atrato	56 ± 7	33	204	34	9	24	−76.7	6.2	Tagachi, Colombia
26	Danube	202 ± 36	166	202	788	807	80	28.7	45.2	Ceatal Izma, Romania
27	Niger	33 ± 9	102	193	2240	1516	29	3.5	11.9	Gaya, Niger
28	Ogooué	148 ± 22	139	186	210	204	42	10.2	−0.7	Lambaréné, Gabon
29	Essequibo	69 ± 15	25	154	151	67	13	−58.6	5.8	Plantain Island, Guyana
30	Fraser	86 ± 11	121	144	245	217	79	−121.4	49.4	Hope, Canada
31	Pechora	135 ± 16	126	140	302	312	36	52.2	67.6	Oksino, Russia
32	Nelson	70 ± 17	84	126	1047	997	34	−97.9	54.8	Upstream of Bladder, Canada
33	Khatanga	78 ± 3	69	124	371	275	13	102.5	72.0	Khatanga, Russia
34	Sepik	119 ± 9	112	123	77	41	4	142.2	−4.2	Ambunti, Papua New Guinea
35	Kolyma	99 ± 26	83	118	666	526	17	158.7	68.7	Kolymskoye, Russia
36	Zambeze	105 ± 44	404	117	1989	940	4	33.6	−16.1	Matundo-Cai, Mozambique
37	Severnaya Dvina	106 ± 20	176	112	367	348	112	41.9	64.1	Ust Pinega, Russia
38	Indus	89 ± 25	125	104	1143	975	31	68.3	25.4	Kotri, Pakistan
39	Sanaga	63 ± 9	65	99	129	132	37	10.1	3.8	Edéa, Cameroon
40	Godavari	97 ± 32	86	97	312	299	74	81.8	16.9	Polavaram, India

TABLE 2. (*Continued*)

No.	Name	Vol at station		River mouth		Stn DA	Nyr	Lon (°)	Lat (°)	Station, Country
		Str ± std dev	RTM	Vol	DA					
41	Rajang	70 ± 10	83	93	56	34	32	112.9	2.0	Kapit Wharf, Malaysia
42	Sao Francisco	89 ± 28	127	90	615	623	56	−37.0	−10.0	Traipu, Brazil
43	Usumacinta	59 ± 12	57	89	68	51	35	−91.5	17.4	Boca del Ce, Mexico
44	Maroni	59 ± 14	11	86	65	64	4	−54.5	5.0	Langa Tabbe, Suriname
45	Rhine	73 ± 14	86	75	165	180	6	6.1	51.8	Lobith, Netherlands
46	Purari	74 ± 13	60	74	34	29	6	145.1	−7.0	Wabo Dam, Papua New Guinea
47	Caniapiscau	43 ± 13	11	73	143	87	31	−69.2	57.4	Chute de la, Canada
48	Mahanadi	60 ± 33	63	73	141	132	6	84.0	20.8	Kaimundi, India
49	Sacramento	21 ± 7	11	69	193	61	31	−121.5	38.6	Sacramento, CA, United States
50	Jacui	55 ± 11	50	69	81	71	5	−51.5	−30.0	Paso do Ra, Brazil
	Total:	17 492 ± 552*	18 079	21 152	50 415	42 364				

* This number, which was estimated as the square root of the sum of the variance of the listed rivers, provides only an estimate for the true std dev of the total volume.

flow dataset is, however, not an easy task. We first created a subset of stations that are not far away from the coastlines using the distance to ocean as the criterion. This subset of coastal stations still included upstream stations for a number of rivers, while some of the large rivers (e.g., Niger, Mekong, Huanghe) were not included because the farthest downstream gauging stations are quite distant from their mouths. We manually deleted the upstream stations.

We assigned a class number (1–6) to each river based on the downstream width (~2/3 weight) and total length (~1/3 weight) of the river shown on the *Times Atlas of the World* (1999 edition; scales, 1 : 1.0–5.5 million) that qualitatively represents the size or magnitude of the river. For example, the Amazon, Congo, Orinoco, and the other top 10 rivers were assigned class 6 (largest rivers), while class 5 (very large rivers) included Tocantins, Yukon, Niger, Rhine, and the other top 50 rivers. Examples of class 4 (large rivers) include Colorado in North America, Murray in Australia, and Taz in Russia. The majority of world rivers are in class 3 (significant rivers, such as Trinity in Texas, Deseado in Argentina, Limpopo in Mozambique), class 2 (small rivers, e.g., San Antonio in the United States, Neepan in Australia, Orne in France), and class 1 (smallest rivers on the map).

Although the merged streamflow dataset is among the most comprehensive available, it was unknown whether it included all the major rivers of the world. Furthermore, we wanted to ensure that we selected all the significant (classes 3–6) ocean-reaching rivers from the merged dataset. For these purposes, we looked through the atlas for all named ocean-reaching rivers on all continents and large islands. If the name of a river from the atlas was not in the subset but found in the merged dataset, then the farthest downstream station for that river was added to the subset of coastal stations.

Through this tedious process, we found out that the merged streamflow dataset included all the class 6 and 5 rivers and most class 4 rivers (except for Cuanza in Angola, and Fuchunjiang and Yalujiang in China). However, a large percentage of the class 3 (~1/3) and class 2 (~1/2) rivers were not in the merged streamflow dataset. Apparently, there have either been no gauging stations or the data have not been released to the international community for these rivers. This is particularly true in Indonesia and other south Asian countries.

For some big rivers, there are significant branch rivers entering the main stream below the farthest downstream stations. For example, Obidos, the farthest downstream station available for the Amazon, is ~750 km away from the mouth. Below Obidos, two very large (Tapajos and Xingu), two large (Jari and Paru), and several class 3 and 2 rivers enter the Amazon. Although these rivers do not reach the ocean by themselves, they are included in our subset of ocean-reaching rivers if station data are available. Another example is the Bénoué (no. 52 in the appendix), which flows into the Niger (no. 27 in Table 2) well below the last gauging station at Gaya in Niger.

The search of a dataset from GRDC containing long-term mean streamflow data for 198 rivers, used by GRDC to estimate freshwater fluxes into world oceans (Grabs et al. 1996), resulted in an addition of four rivers to our subset of ocean-reaching rivers.

Finally, we selected 921 ocean-reaching rivers (including those entering the Mediterranean and Black Seas), whose station locations are shown in Fig. 1 together with a simulated network of the world's major river systems (by the river transport model described below). While the coasts in North and South Americas and Europe are well monitored, there are large river systems not monitored in tropical Africa and south Asia. Australia is a relatively dry continent and there is an absence of rivers along the southern coastline, so the network there appears to be sufficient.

b. Estimating continental discharge

1) DISCHARGE BASED ON STATION DATA

To estimate continental discharge into each ocean basin at each latitude from the station data of streamflow, one can sum up the river outflow within each latitude band for each ocean basin. Before this can be done, however, we need to estimate the streamflow at the river mouth from the coastal station data and the contributions from rivers (or drainage areas) that are not monitored by the stations.

Although most of the selected coastal stations are close to river mouth, it is rare that a gauging station is right on the coast. For many rivers (e.g., Niger, Mekong, Amazon), the farthest downstream stations available are quite distant from the coast and thus streamflow measurements are not representative of the actual outflow into ocean. Although including the contributions separately from the rivers that enter downstream partly solves the problem (e.g., for Amazon), many downstream rivers are not monitored.

We used an RTM to estimate river mouth outflow from the upstream station data. The RTM was developed by M. L. Branstetter and J. S. Famiglietti and is described by Branstetter (2001) and Branstetter and Famiglietti (1999). The RTM is used in the NCAR Community Climate System Model (CCSM; Blackmon et al. 2001) for routing surface runoff into the oceans. Using a linear advection scheme at 0.5° resolution, the RTM routes water from one cell to its downstream neighboring cell by considering the mass balance of horizontal water inflows and outflows (Branstetter 2001):

$$\frac{dS}{dt} = \sum F_{\text{in}} - F_{\text{out}} + R, \qquad F_{\text{out}} = \frac{v}{d}S, \qquad (1)$$

where S is the storage of stream water within the cell (m^3), F_{out} is the water flux leaving the cell in the downstream direction ($m^3\ s^{-1}$), ΣF_{in} is the sum of inflows of water from adjacent upstream cells ($m^3\ s^{-1}$), R is the runoff generated within the cell ($m^3\ s^{-1}$), v is the effective water flow velocity [$=0.35$ m s^{-1}, following Miller et al. (1994)], and d is the distance between centers of the cell and its downstream neighboring cell (m).

The water flow direction is one of eight directions chosen as the downstream direction for each cell, based on the steepest downhill slope. Note that stream channel losses to groundwater recharge, reservoirs, and irrigation are not included in this version of the model. Tests showed that the choice of v only affects the time for the model to reach an equilibrium under a constant runoff field. This time is about 6 months with $v = 0.35$ m s^{-1} (for the Amazon) starting from empty river channels. We used the river flow rates after 200 model days in annual simulations, and used the data of the second year in monthly simulations.

To simulate the annual-mean streamflow of the world river systems, we forced the RTM with the annual runoff from Fekete et al. (2000, 2002). In general, this simulation, which was run with daily time steps, produced comparable river flows at the coastal stations of most major rivers (see Table 2 and the appendix). We used the ratio of the simulated streamflow at the river mouth to that at the farthest downstream station to scale up (on monthly and annual timescales) the observed station flow as the river mouth outflow (vol in the tables) for the world's top 200 rivers listed in Table 2 and the appendix. In some cases (e.g., no. 23 Uruguay and no. 29 Essequibo in Table 2), where this simulated-flow ratio was unreasonable (<0.9, or >2.0 except for Niger), we instead used the ratio of drainage areas (based on STN-30p) at the river mouth to that at the station for the scaling. The estimated river mouth outflow was then used to compute continental discharge. All branch rivers above the mouth of the main river channel were excluded in this calculation. These excluded branch rivers are no. 12 Tapajos, no. 18 Xingu, no. 52 Bénoué, no. 60 Chindwin, no. 89 Red, no. 105 Jari, and a few smaller rivers. For other smaller rivers, not listed in Table 1 and the appendix, station streamflow was treated as river mouth outflow and used in estimating continental discharge. The use of the river mouth outflow increases the estimates of the global continental discharge by 18.7% and the total monitored drainage area by 20.4%.

The total drainage area monitored by the 921 ocean-reaching rivers (at river mouths) is 79.5×10^6 km^2, which accounts for about 68% of global nonice, nondesert land areas [$\approx 117 \times 10^6$ km^2; Dai and Fung (1993)]. Therefore, approximately one-third of the world's actively drained land area is not monitored by the available gauging stations. Earlier studies (e.g., Marcinek 1964) estimated runoff from these unmonitored areas on the basis of comparable regions (i.e., nearby regions having runoff data). Fekete et al. (2000) showed that simply using the ratio of global actively drained area to the monitored area to scale up the global continental discharge estimate resulted in a number (28 700 $km^3\ yr^{-1}$) that was too low compared with other esti-

TABLE 3. The ratio of mean runoff between unmonitored and monitored river basins for each receiving ocean basin and the global ocean. The monitored basins used in this calculation consist of the world's largest 243 rivers with a total drainage area of 69.8×10^6 km^2, or about 59.7% of the total area of actively drained landmass. The global ocean includes the Mediterranean and Black Seas. Also shown (A_u/A_m) is the ratio of unmonitored to monitored (by the 921-river network) drainage areas.

	Runoff ratio					Area ratio
	Jan	Apr	Jul	Oct	Annual	A_u/A_m
Arctic Ocean	1.514	0.918	1.169	1.634	1.051	0.331
Atlantic Ocean	0.664	0.885	1.167	1.347	0.931	0.300
Indian Ocean	1.158	1.427	0.293	0.336	0.525	1.323
Mediterranean and Black Seas	1.599	2.790	0.556	0.534	1.191	0.735
Pacific Ocean	4.301	2.350	1.691	2.529	2.300	0.535
Global ocean	1.146	1.000	0.938	1.267	1.022	0.507

mates. Perry et al. (1996) used a power law size distribution found for large rivers to estimate the total contribution from all small rivers.

Here we made use of the ratio of runoff (based on Fekete et al. 2000) between unmonitored and monitored areas to account for the contribution of the unmonitored areas to continental discharge using the following formula:

$$R(j) = R_0(j)[1 + r(j)A_u(j)/A_m(j)], \quad (2)$$

where $R(j)$ is the continental discharge for 1° latitude zone j (for individual ocean basins), and $R_0(j)$ is the contribution from the monitored areas only (i.e., the sum of river mouth outflow for all rivers with data within latitude zone j); $A_u(j)$ and $A_m(j)$ are the unmonitored and monitored drainage areas, respectively, whose runoff enters ocean in latitude zone j (i.e., A_u and A_m may be outside latitude zone j), and $r(j)$ is the ratio of mean runoff over A_u and A_m. Equation (2) was first applied to individual ocean basins. To create the discharge from individual 1° coastal boxes, the contribution from A_u was further partitioned into the individual coastal boxes within the 1° latitude zone j for each ocean basin based on the allocation of A_u on the coasts. For display purposes, the 1° discharge was aggregated onto a 4° latitude × 5° longitude grid. Note that there are inconsistencies in Table 2 and the appendix between the two drainage areas listed, as the station drainage area comes from the station datasets while the river mouth drainage area comes from STN-30p; presumably the latter should be greater.

In this calculation, the coastal outflow location for the runoff generated over each 0.5° land cell was first derived based on STN-30p, and the runoff over A_u is put into the ocean at the correct location. Here, $r(j)$ was computed using monthly and annual runoff fields from Fekete et al. (2000). It was found necessary to smooth $r(j)$ over 4° latitude zones, because for narrower zones A_m can be zero or small. These $r(j)$ values were then used in monthly and annual calculations of $R(j)$ at 1° latitude resolution. Typical values of $r(j)$, together with $A_u(j)/A_m(j)$, averaged over the drainage area of each ocean basin, are shown in Table 3. The value of $r(j)$ varies from 0.29 for the Indian Ocean in July, owing to very dry unmonitored regions in the summer monsoon, to 4.30 for the Pacific Ocean in January, where the unmonitored wet regions of Indonesia come into play. For the global land areas, however, this ratio is close to one, which supports the notion that the unmonitored landmass as a whole is unlikely to be significantly wetter than the monitored land areas (Fekete et al. 2000). Table 3 also shows that the drainage areas into the Atlantic and Arctic oceans are well monitored by the 921 river network, while the monitoring network is poor for the Indian Ocean [partly due to large unmonitored arid areas where $r(j)$ is small and thus has little effect on $R(j)$; cf. Fig. 1]. Globally, the unmonitored areas (including arid regions) account for about half of the monitored areas, or one-third of the total drainage areas.

Implicit in our approach is that we are dealing with the actual flows into the oceans, not the natural flows that would occur without dams and other interference by humans. This aspect does causes complications because comparisons with climate models that do not include or allow for effects of human interference should expect discrepancies. The gauge records reflect the actual flow, regulated or not, and as this may well have changed over time, the more recent records may differ from those of previous decades. Moisture from irrigation can be evaporated, which should be reflected in measurements of atmospheric moisture and thus in our P–E estimates.

Compared with earlier studies, our method for estimating the discharge from the unmonitored areas has some unique features that should improve our station-data-based estimate of continental runoff. For example, it makes use of runoff information over the monitored and unmonitored areas. It also integrates the runoff from the unmonitored areas and puts it into oceans at correct locations with the help of the river database. Most earlier studies merely scale up the global total discharge derived from the monitored areas and fail to do this geographically.

2) DISCHARGE BASED ON RUNOFF FIELDS

Continental discharge can also be estimated based on runoff fields. BR75 used the runoff field (in mm) derived

by Marcinek (1964) to estimate continental discharge for each 5° latitude zone using simple areal integration. However, as many large rivers (e.g., Mississippi, Paraná, Nile, Niger, and most Russian rivers) flow mostly north–south, simple zonal integration of runoff does not provide correct estimates of continental discharge for a given latitude zone.

A substantial advance can be made by using the RTM to route the excess water (runoff) within each 0.5° cell into the ocean and then estimate continental discharge by totaling the simulated coastal river outflows within each 1° latitude zone. Maps of coastal discharges at 1° and 4° latitude × 5° longitude resolution were obtained from the RTM simulations. Three different runoff fields were used: (i) the composite runoff fields of Fekete et al. (2000), and runoff estimated using the multiyear mean monthly and annual *P–E* fields from the (ii) NCEP and (iii) ECMWF reanalyses (Table 1). Daily runoff was interpolated from monthly mean fields and used to drive the RTM. These discharge estimates provide additional checks for the gauge-based estimate, as well as an evaluation of the reanalysis *P–E* fields.

Fekete et al. (2000) simulated snow accumulation and melt using some simple empirical equations in producing the composite runoff. We adopted a simple scheme from Haxeltine and Prentice (1996) to simulate the effects of snow on runoff in using the monthly *P–E* from the reanalyses for driving the RTM. The climatological daily surface air temperature (t_d in °C), interpolated from the monthly climatology of New et al. (1999), is compared with a constant t_s. When $t_d < t_s$, then positive *P–E* accumulates as snowpack and runoff is zero; if $t_d > t_s$, then snow melts at a rate sm (mm day^{-1}) $= k\,(t_d - t_s)$, where k is a constant in millimeters per (day °C). Haxeltine and Prentice (1996) used −2.0°C for t_s and 0.7 for k. We tested a number of values for these two parameters in order to produce the best match between the simulated and observed annual cycle of continental discharge and selected 0.0°C for t_s, which is physically reasonable, and 0.7 for k. In reality, of course, temperatures vary considerably within a month, so that even if the monthly mean is less than 0°C, several days could be above that threshold, but the simplification we use is consistent with the other shortcomings in approximating runoff by mean *P–E*, rather than employing hourly, or at least daily, data to properly deal with issues discussed in the introduction.

4. Comparison among runoff estimates

To help understand discharge differences discussed below, we first compare annual means of the Fekete et al. runoff and the *P–E* derived from the NCEP and ECMWF reanalyses. Figure 2 shows the annual-mean runoff from Fekete et al. (2000), the *P–E* fields, and the mean precipitation (average of CMAP and GPCP) (left column), together with the implied *E* (i.e., the precipitation minus the runoff or *P–E*) and the difference between the NCEP and ECMWF *P–E* (right column). First, both the NCEP and ECMWF *P–E* fields show negative values over many regions of all continents, especially in central and western Asia and northern Africa. While it is physically possible to have negative *P–E* over land (e.g., due to water flowing into the region, groundwater mining, and evaporation from reservoirs and lakes), negative *P–E* cannot be used as runoff. Some of these regions indicate deficiencies in *P–E* arising from insufficient atmospheric observations (especially in Africa). We set the negative annual *P–E* to zero in forcing the RTM. The negative *P–E* over many coastal areas, such as eastern Africa, appears to result from extensions of oceanic *P–E* patterns. This problem may stem from the relatively low horizontal resolution of the reanalysis *P–E*. On the other hand, some regions, such as southern California, are heavily irrigated using, for instance, water from aqueducts. As a result, negative *P–E* values are plausible.

Second, the implied *E* for both the *P–E* fields and, to a smaller extent, the Fekete et al. runoff, has negative values over a number of land areas. Some of these negative values of *E* suggest that the Fekete et al. runoff and the *P–E* are too large since the CMAP and GPCP precipitation climatologies are generally reliable over nonmountainous land areas and they cover similar data periods (Table 1). These areas with negative *E* (especially nonmountainous areas), together with those land areas with negative *P–E* for the reanalyses cases, contribute to errors in estimating continental freshwater discharge.

Third, substantial differences exist on regional scales over both land and ocean between the *P–E* fields derived from the NCEP and ECMWF reanalyses, even though the large-scale patterns are comparable. While the difference patterns are noisy, the NCEP *P–E* is generally lower than the ECMWF *P–E* over the southern subtropical (20°–40°S) oceans, the eastern Pacific and the Atlantic around 3°–12°N, and much of the western North Atlantic. Over the continents, the NCEP *P–E* also has a dry bias compared with the ECMWF *P–E*. On the other hand, the ECMWF ERA-15 reanalysis data have a major problem over Africa, namely a spurious southward shift of the intertropical convergence zone (ITCZ) after 1987 (Stendel and Arpe 1997; Trenberth et al. 2001b).

The implied *E* fields are spatially correlated with the precipitation field, with the correlation coefficient r ranging from 0.66 to 0.79 over land and slightly lower over ocean for the reanalysis cases. This is expected since precipitation provides the main water source for evaporation over most land areas.

5. Freshwater discharge from the world's major rivers

Table 2 and the appendix present the annual-mean river flow rate and drainage area at the farthest down-

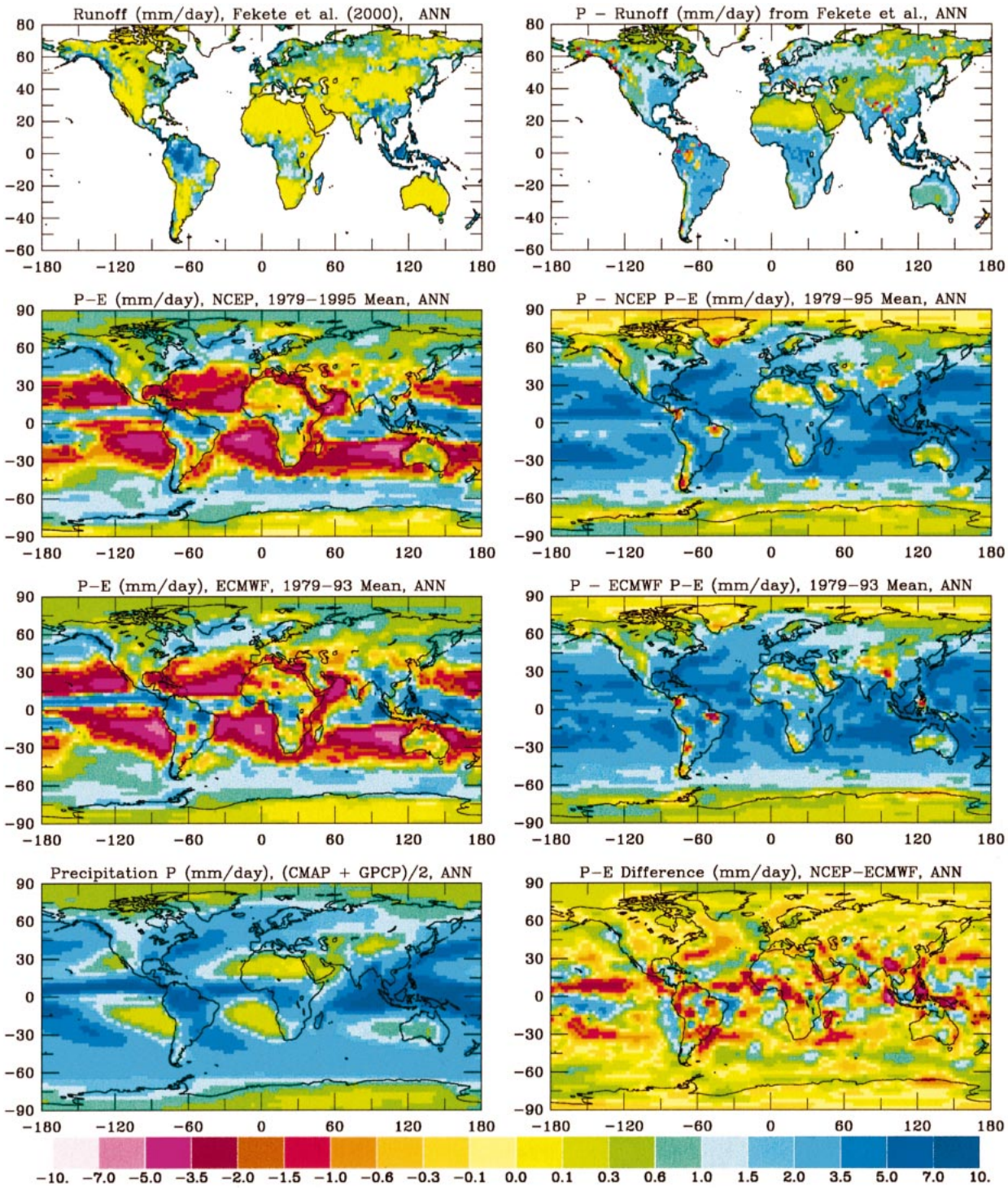

FIG. 2. Annual runoff from Fekete et al. (2000), *P–E* derived from the NCEP and ECMWF reanalyses, mean precipitation of CMAP and GPCP (left column), and the implied *E* (i.e., *P*–runoff or (*P–E*)] and the NCEP − ECMWF difference of *P–E* (right column).

stream station and the river mouth for the world's largest 200 rivers. The river mouth flow was estimated using the method described in section 3b. The drainage area at the river mouth was estimated using the river database STN-30p. The river flow simulated at the station by the RTM forced with the annual runoff field of Fekete et al. (2000) is also shown next to the observed volume.

Many of the world's largest river systems, with the

TABLE 4. Comparison of estimates of mean annual continental freshwater discharge into the individual and global oceans ($km^3\ yr^{-1}$).

	Arctic	Atlantic	Indian	Mediterranean Sea[c]	Pacific	Total[d]
Largest 921 rivers[a]	3658	19 168	4532	838	9092	37 288
Fekete runoff	3263	18 594	5393	1173	10 420	38 843
ECMWF *P–E*	3967	20 585	4989	1144	7741	38 426
NCEP–NCAR *P–E*	4358	16 823	3162	909	7388	32 640
Fekete et al. (2000)	2947	18 357	4802	1169	11 127	38 402
Korzun et al. (1977)[b]	5220	20 760	6150		14 800	46 930
Baumgartner and Reichel (1975)	2600	19 300	5600		12 200	37 713
Oki (1999)	4500	21 500	4000		10 000	40 000

[a] Largest 921 rivers are scaled up by accounting for the unmonitored areas and the runoff ratio at 4° lat resolution.
[b] Korzun et al. (1977) include groundwater runoff (2200 $km^3\ yr^{-1}$ globally) and iceberg runoff (2700 $km^3\ yr^{-1}$ globally).
[c] Mediterranean Sea includes the Mediterranean and Black Seas.
[d] Total excludes discharge into inland (besides Black) seas and from Antarctica, which puts ~2613 $km^3\ yr^{-1}$ freshwater into the ocean (Jacobs et al. 1992).

exception of the Yenisey, Lena, Ob, and Amur, are located at low latitudes, where precipitation rates are highest. River discharge in general increases with drainage area, but the river flow to drainage area ratio varies from about 1 $km^3\ yr^{-1}$ per 1000 km^2 in the Tropics (equivalent to *P–E* of 1 m yr^{-1}) to less than 0.1 $km^3\ yr^{-1}$ per 1000 km^2 in high latitudes and dry areas.

The total global freshwater discharge, excluding that from Antarctica, is about 37 288 ± 662 $km^3\ yr^{-1}$ (Table 4), which is ~7.6% of global precipitation or 35% of terrestrial precipitation (excluding Antactica and Greenland) based the averaged precipitation of CMAP and GPCP. Since a time series of global discharge is not easy to derive because of a changing number of gauges, this uncertainty range was estimated as the square root of the sum of the variance of long-term mean annual flows at the farthest downstream stations of all the 921 rivers multiplied by 1.187, the global-mean factor for converting the farthest downstream station flows to the river mouth outflows. Hence it is based on the assumption that the covariance of streamflow among large rivers is small. The world's 50 largest rivers (Table 2) account for ~57% of the global discharge, while their total drainage area is ~43% of the global actively drained land areas (i.e., excluding glaciers and deserts). Adding the next 150 largest rivers (the appendix) increases these to 67% and 65%, respectively, while adding the next 721 rivers in our dataset of coastal stations changes the numbers only moderately (to 73% and 68%, respectively). This suggests that an increasingly large number (in the thousands) of smaller rivers are needed to improve the coverage of the station network for monitoring global freshwater discharge.

Table 2 and the appendix show that the farthest-downstream station data underestimate—by 10% to over 100%—the river discharge and drainage area at the river mouth in many cases (e.g., Amazon, Orinoco, Mississippi, Paraná, Mekong, Irrawaddy, St Lawrence, and Niger). Most earlier estimates of streamflow and drainage area for the world's largest rivers used unadjusted data from the available farthest downstream station (e.g., Probst and Tardy 1987; Perry et al. 1996; Grabs et al. 1996, 2000). These unadjusted estimates not only underestimate the true river outflow, but also contribute to the large range among various estimates of flow rate for world's major rivers because the distance from the farthest downstream station to the river mouth varies among different studies from hundreds to thousands of kilometers (Perry et al. 1996). For example, Perry et al. (1996) listed the Amazon with a mean flow rate of 6088 ± 465 (std dev) $km^3\ yr^{-1}$ based on 11 different sources, while it is 6000 $km^3\ yr^{-1}$ in BR75. Although these are higher than our mean flow rate (5330 $km^3\ yr^{-1}$) at station Obidos, they are about 10% lower than our estimate of Amazon mouth flow (6642 $km^2\ yr^{-1}$).

When forced with the annual runoff from Fekete et al. (2000), the RTM simulates the station flow rates reasonably well for most major rivers (Fig. 3a, also see Table 2 and the appendix). This suggests that both the Fekete et al. runoff and the RTM routing scheme are likely to be correct over most regions. However, problems are evident over a few river basins such as the Nile (no. 83) and Zambeze (no. 36), where the RTM greatly overestimates the river channel flow. For the Nile, river channel water losses due to evaporation and human withdrawal contribute to the smaller-than-simulated flow rate. The drainage areas derived from the STN-30p are close to those given in the station datasets (Fig. 3b), except for a few cases (e.g., Zambeze) where drainage areas from the streamflow datasets are likely to be incorrect, as the STN-30p provides one of most reliable estimates for the total drainage areas of world's largest rivers.

When the RTM is forced by the *P–E* fields derived from the NCEP and ECMWF reanalyses, the simulated station flow rate generally agrees with the observed at most of the major rivers (Fig. 4). Substantial differences exist, however, for the world's largest rivers. For example, the simulated flow rate is 3063 and 3833 $km^3\ yr^{-1}$ for the Amazon at Obidos in the NCEP and ECMWF cases, respectively, where the observed rate is 5330 $km^3\ yr^{-1}$. In general, the Fekete et al. runoff re-

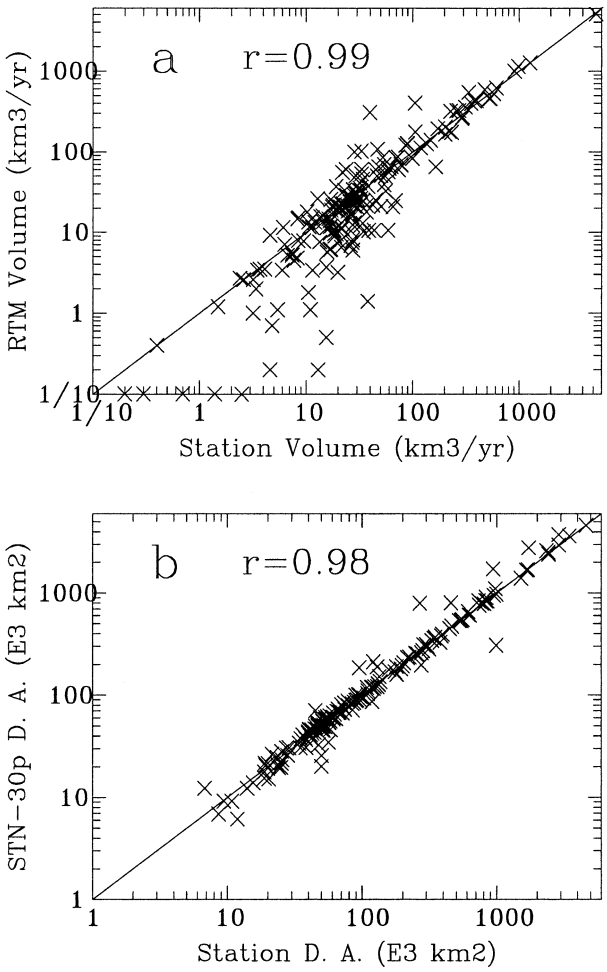

FIG. 3. (a) Observed (*x* axis) vs RTM-simulated annual river flow and (b) the drainage area from the streamflow datasets and from the simulated river network STN-30p at the farthest downstream stations for the world largest 200 rivers listed in Table 1 and the appendix. The annual runoff field from Fekete et al. (2000) was used in the RTM simulation. The *r* is the correlation coefficient of the data points. Note that both of the coordinates are on a logarithmic scale.

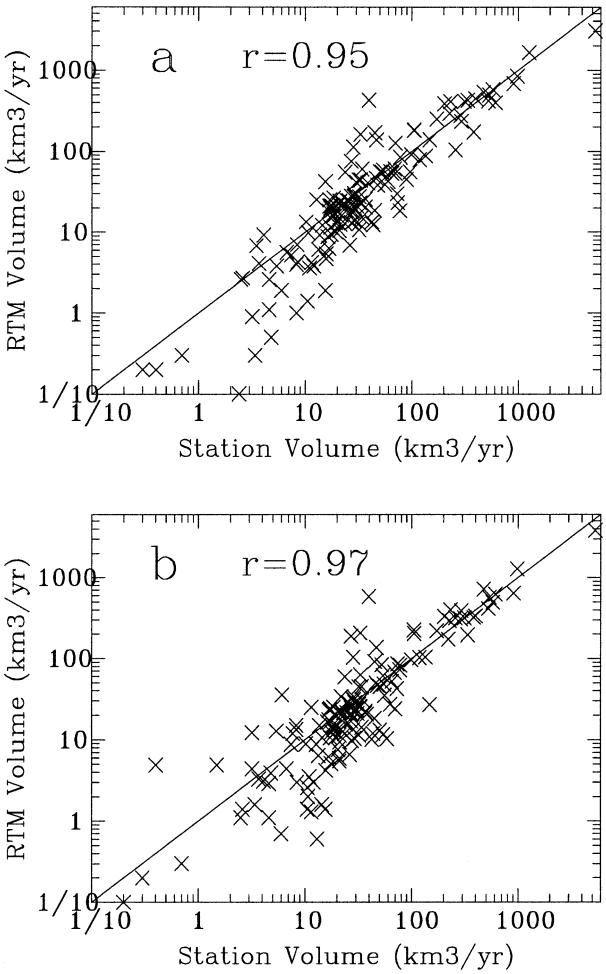

FIG. 4. Same as in Fig. 3a but with the RTM forced by the *P–E* fields derived from the (a) NCEP and (b) ECMWF reanalyses.

sulted in better simulated station flow rates, especially for the world's largest rivers.

The third column in Table 2 and the appendix lists the standard deviation (std dev) of year-to-year variations of river flow rate at the farthest downstream station. It can be seen that for the large rivers the std dev is ~10%–30% of the mean flow. This ratio increases to over 100% for smaller rivers (the appendix), suggesting that streamflow rates of small rivers are much more variable from year to year than those of large rivers. This result arises because river flow rates are areal integrals of surface runoff and an integral over a larger basin is usually less variable than one over a smaller region.

The streamflow of many rivers has a large annual cycle. Figure 5 compares the mean annual cycle of discharge (thick, solid curve) with those of basin-integrated precipitation (thin, solid curve), runoff, and *P–E* for the 10 largest rivers. Note that the RTM is not used in these basinwide summation and therefore the differences between the river discharge and the basin-integrated values illustrate the effects of snow and the time delay of water traveling downstream to the river mouth. The Amazon has the highest flow from May to June, while its basin-integrated precipitation, runoff, and *P–E* peak in early spring. This lag reflects the time needed for surface runoff to travel to the river mouth. For the Changjiang, Brahmaputra/Ganges, Mississippi, Mekong, and smaller rivers, this time lag is shorter (about 1 month or less), suggesting that the seasonal changes in surface runoff occur in the area not far away from the river mouth. The Congo and Paraná have relatively small annual cycles, even though precipitation and runoff (for Paraná only) exhibit large seasonal variations. There are several reasons for this to happen. First, evaporation positively correlates with precipitation and thus reduces the seasonal variation of surface runoff, which is the case for the Congo. Second, for large rivers like the Paraná,

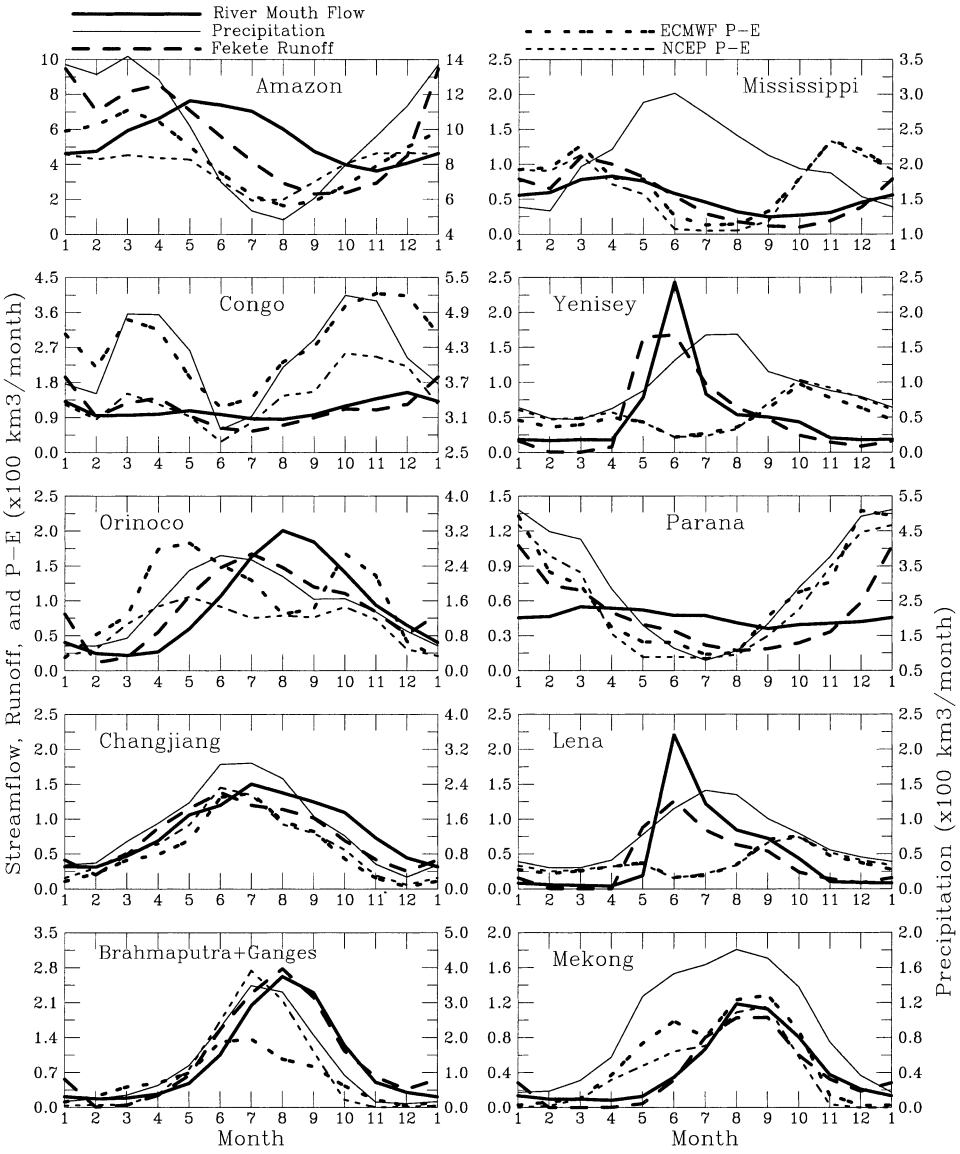

FIG. 5. Mean annual cycle of river discharge, river-basin-integrated precipitation (read on the right ordinate), runoff, and reanalysis *P–E* for world largest 10 rivers. Note that the RTM was not used for this plot.

which runs through different climate zones, regional variations of surface runoff within the river basin, combined with the time lag due to river channel transport, tend to compensate and thus reduce the seasonal variation of downstream river flow. More fundamentally, the relative uniformity of river flows throughout the year in spite of large precipitation variations is a sign of large and diverse lags and obstructions, such as lakes, that help smooth out and regulate the flow.

The big Russian rivers (Yenisey, Lena, Ob, etc.) have large peak flows in June, which result from spring (April–May) snowmelt as precipitation does not peak until July–August in these regions (Fig. 5). In fact, the drainage-area-integrated discharge and precipitation for the entire Arctic region (cf. Fig. 12; also see Grabs et al. 2000) are very similar to those for Yenisey and Lena (Fig. 5). Early spring snowmelt over the Mississippi basin also appears to be the main reason for the April peak discharge from the Mississippi, whose integrated precipitation peaks in May–June.

At low latitudes, the basin-integrated *P–E* generally agrees with the Fekete et al. runoff, indicating that the monthly *P–E* fields are reasonable proxies of monthly runoff provided the areas are large enough. One exception is the ECMWF *P–E* over the Congo River basin, where it follows the precipitation annual cycle rather than the runoff (Fig. 5). This bias is reflected in the high values of *P–E* in tropical Africa (Fig. 2) and is mainly

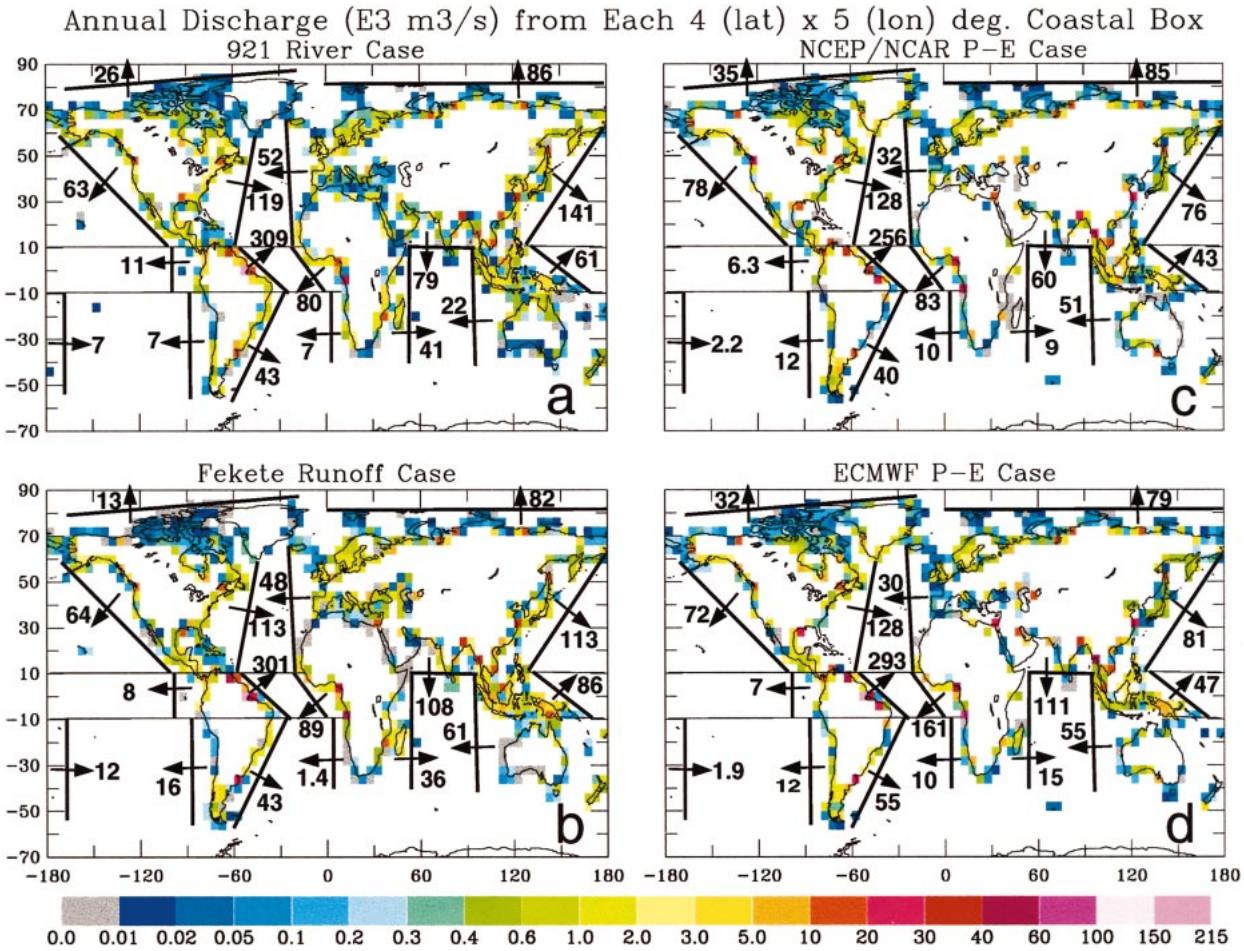

FIG. 6. Annual discharge rate (10^3 m^3 s^{-1}) from each 4° lat by 5° lon coastal box. The numbers are the total discharge (in 10^3 m^3 s^{-1}) from the coasts behind the solid lines. Blank coastal boxes have zero discharge.

due to the higher-than-observed precipitation in the ECMWF data resulting from the spurious ITCZ shift over Africa noted earlier. As noted, spring snowmelt results in peak river flows in late spring or early summer at northern mid- and high latitudes. It also disrupts the general agreement between surface runoff and the *P–E* seen at low latitudes. This suggests that on a monthly timescale the *P–E* fields at mid- and high latitudes cannot be used as a proxy of runoff without including the effects of snow accumulation and melt.

6. Latitudinal distribution of discharge into the oceans

In this section, we consider the continental discharge from the ocean perspective, with a view toward their use in oceanic freshwater transport and budgets. We start from the total discharge into the global ocean and then discuss individual ocean basins separately, with a focus on the latitudinal distribution.

a. Global ocean

Figure 6 shows four estimates of annual freshwater discharge rates from individual 4° latitude × 5° longitude coastal boxes. Also shown are the total discharge (in 10^3 m^3 s^{-1}) from the coasts behind the solid lines.[2] As described in section 3b, these estimates were derived using long-term mean streamflow data from 921 rivers through Eq. (2), the composite annual runoff from Fekete et al. (2000), and the multiyear-averaged *P–E* fields from the reanalyses (see Table 1).

As indicated by the scale of the color bar, coastal discharge rates vary from <10 to 215 000 (at the Amazon mouth) m^3 s^{-1} per 4° × 5° box. Most of the global discharge comes from the world's major rivers, whose mouths are indicated by the boxes in warm colors in Fig. 6a. The eastern coasts of the Americas, primarily

[2] Note that the sum of these numbers differs slightly from that listed in Table 4 due to the use of a different (scale dependent) drainage-basin mask for the coastal integration.

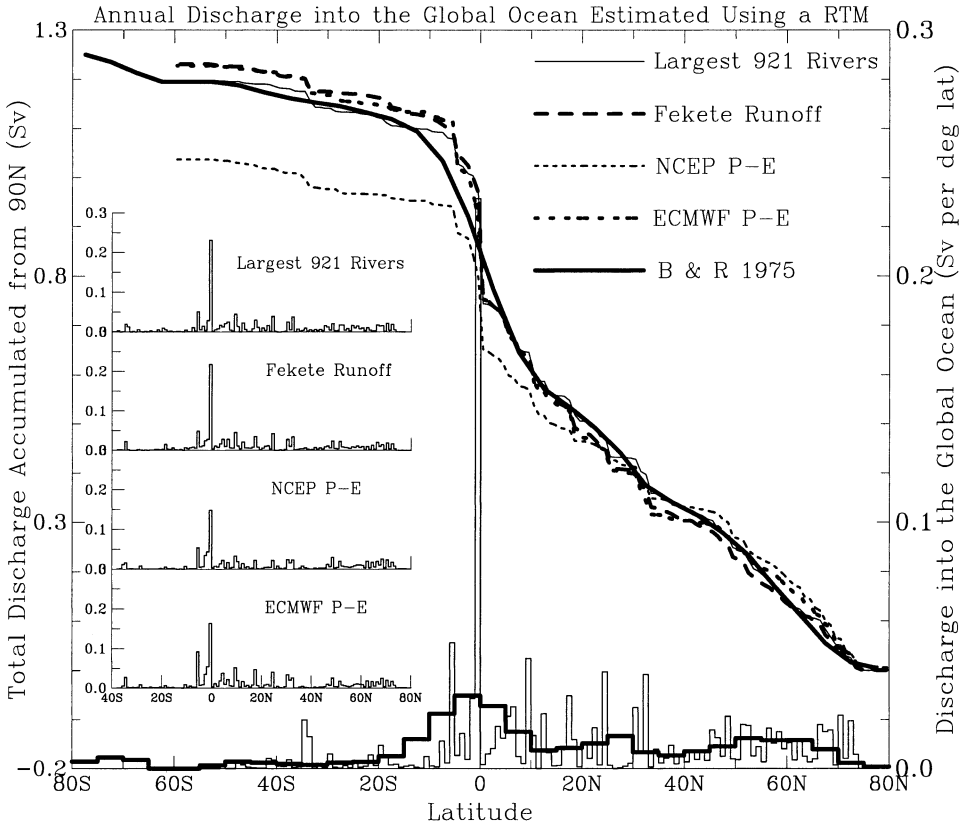

FIG. 7. Estimates of annual mean continental freshwater discharge into the global oceans for each 1° lat zone (right ordinate, lower stepwise lines and the inset) and the cumulated discharge starting from 90°N (upper curves). Each line pattern represents an estimate based either on the largest 921 rivers (thin solid line) or on a runoff field (dashed lines), which was used to force a river transport model to derive the discharge. Also shown is an estimate from Baumgartner and Reichel (1975, thick, solid line).

in the Tropics, provide ~40% of global discharge (Fig. 6a). Discharge from east Asia into the North Pacific accounts for another ~15% of the total. However, less than 10% of the global discharge comes from the western coast of South America.

While the coastal boxes show the approximate locations of the discharge, it is difficult to compare the discharges among the four cases for each grid box in Fig. 6. The integrated coastal discharge provides an easier measure for comparison. It can be seen that the Fekete et al. runoff implies discharges comparable to the river-based estimates from most of the coastlines except for those from east Asia (too low), Indonesia, the Bay of Bengal, and the tropical west Pacific islands (too high) (Fig. 6b). The ECMWF *P–E* implied discharges are also similar to the river-based estimates, except for the coasts of east Asia, western Australia, and Africa (Fig. 6d). The NCEP case reproduces the discharge into the Arctic, South Atlantic, and South Pacific Oceans, but has large deficiencies over eastern Africa, Europe, and east Asia (Fig. 6c). In general, both the ECMWF and NCEP cases underestimate discharges from northern Africa and east Asia, largely due to the negative values of *P–E* (which was set to zero in the RTM simulations) over these regions (cf. Fig. 2).

Figure 7 shows the annual-mean continental freshwater discharge into the global oceans for each 1° latitude zone (stepwise lines) and the discharge accumulated starting from 90°N (upper curves). For comparison, the estimate by BR75 is also shown (thick, solid line). As expected, the continental discharge is dominated by the peak outflows from the world's largest rivers such as the Amazon (~0.21 Sv at 0.75°S, 1 Sv $= 10^6$ m^3 s^{-1}), Congo (0.041 Sv at 5.75°S), Orinoco (0.036 Sv at 9.25°N), Changjiang (0.030 Sv at 32.25°N), Brahmaputra/Ganges (0.033 Sv at 24.25°N), Mississippi (0.019 Sv at 30.25°N), and Paraná (0.018 at 34.75°S) (note that the peaks in Fig. 7 may exceed these numbers because of contributions from small rivers within the same latitude band). The northern mid- to high latitudes (45°–75°N) encompass the largest landmass and many large rivers, including the Yenisey, Lena, Ob, and Amur in Russia; Mackenzie and St. Lawrence in Canada; and Yukon in Alaska. Many of the Russian and Canadian rivers run from south to north and enter the Arctic Ocean. Collectively, these rivers provide a large fresh-

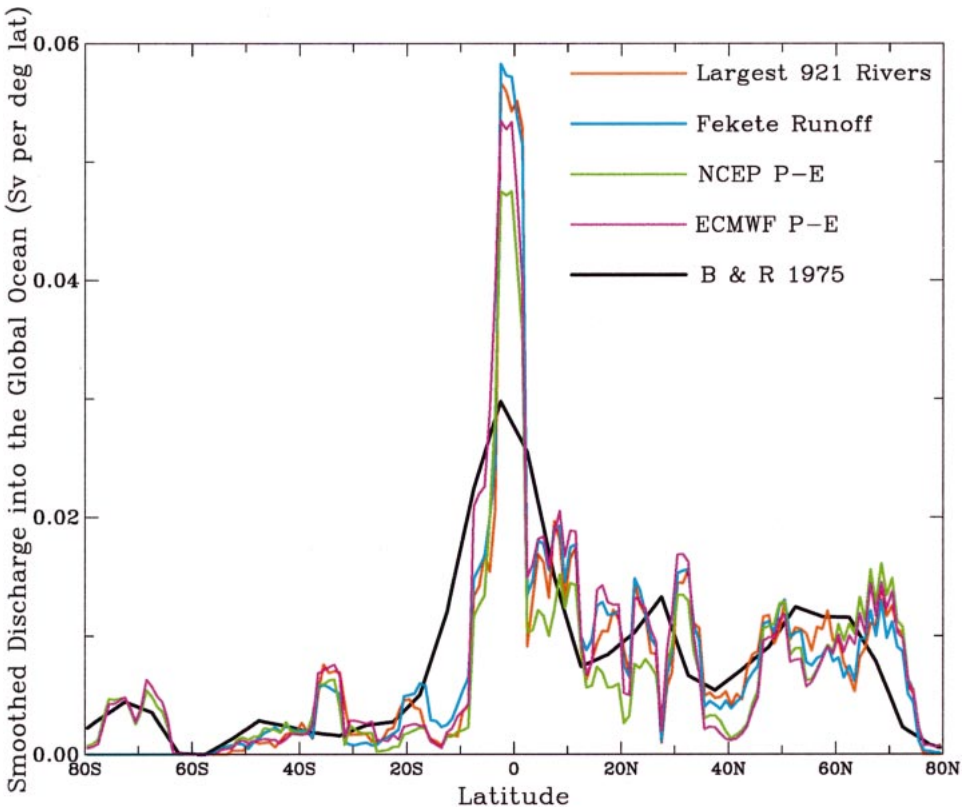

FIG. 8. Annual discharge into the global ocean smoothed using a 5° lat running mean from four different cases, compared with that of Baumgartner and Reichel (1975).

water discharge into the Arctic, North Atlantic, and North Pacific Oceans (cf. Fig. 2), thereby affecting the oceanic water budget and circulation, both locally and globally, especially through the thermohaline circulation. Since the northern mid- and high latitudes are expected to have the largest temperature and precipitation increases in the next 100–200 yr due to increases in CO_2 and other greenhouse gases (e.g., Dai et al. 2001a,b), it is vital to establish an observed baseline.

The RTM reproduces the peak outflows from the world's largest rivers when forced with the Fekete et al. runoff and the reanalysis *P–E* fields, although the magnitude of the peaks differ somewhat from the estimates based on observations (see the insert in Fig. 7, also see Table 2). These differences are also shown by the accumulated discharges. Note that the accumulated discharge, a common measure used in previous studies (e.g., Wijffels 2001), integrates the errors from 90°N southward, and the differences at southern latitudes do not reflect the actual errors at those latitudes because contributions are small south of 10°S.

The accumulated discharge for the NCEP *P–E* case is considerably lower than the others, whereas the BR75 case agrees remarkably well with our estimates based on the streamflow data, Fekete et al. runoff and ECMWF *P–E*. However, the latitudinal distribution from BR75 at 5° resolution is too smooth and quite unrealistic. Even after smoothing the 1° discharge data using 5° latitude running-mean, large differences still exist between the BR75 and our estimates, whereas the agreement among our four different estimates improves (Fig. 8).

The total continental discharge into the oceans is also of interest for the global water cycle. This flux is often estimated by totaling the discharge from the world's major rivers and then adjusting it to account for the contribution from the unmonitored smaller rivers. As discussed in section 3b, our method for estimating the discharge from the unmonitored areas makes our river-based estimate of continental discharge much more reliable than in earlier studies (e.g., BR75; Perry et al. 1996).

Table 4 compares our estimates of total freshwater discharge into the ocean basins with four earlier estimates. Discharge from groundwater, which was estimated to be around 5% of the total discharge by Lvovich (1970), is included only in the estimates using the *P–E* data and from Korzun et al. (1977). Small surface freshwater discharge from Antarctica (=1987 $km^3\ yr^{-1}$ according to BR75) and changes in land storage (e.g., effects of melting glaciers, discussed in section 1) are also not included. Our 921-river-based estimate of the global discharge is 37 288 ± 662 $km^3\ yr^{-1}$ (1 $km^3\ yr^{-1}$ = 31.69 $m^3\ s^{-1}$), which is very close to that of BR75 (37 713) and Perry et al. (1996) (37 768). However,

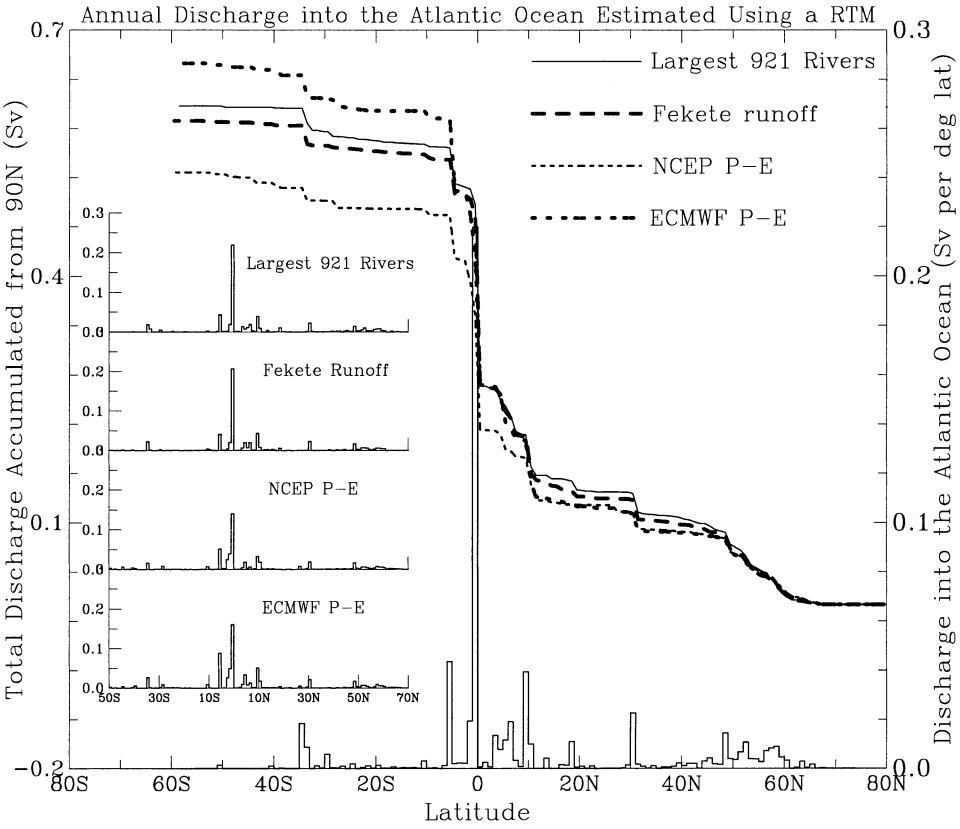

FIG. 9. Estimates of annual-mean continental freshwater discharge into the Atlantic Ocean for each 1° lat zone (right ordinate, lower stepwise lines and the inset) and the cumulated discharge starting from 90°N (upper curves).

Perry et al. (1996) used streamflow rates from the farthest downstream stations, which underestimate the true river discharge by an average of 18.7% in our analysis (see Table 2 and the appendix). This result implies that the power law size distribution used by Perry et al. (1996) substantially overestimates the total discharge from small rivers with an annual flow rate <250 m^3 s^{-1}.

The global discharge implied by the Fekete et al. runoff and ECMWF *P–E* is only slightly higher than that based on streamflow data, while the NCEP *P–E* results in lower global discharge (Table 4), consistent with the dry bias (cf. Fig. 2). This result suggests that the ECMWF ERA-15 *P–E* is likely to be more reliable over global land than the NCEP *P–E* and it may be considered as a proxy for terrestrial runoff for estimating continental discharge, although problems exist in Africa and South America.

Although the various estimates of total continental discharge listed in Table 4 are in good agreement, except for Korzun et al. (1977), their partitioning of the total discharge into individual ocean basins differs substantially. For example, compared with the 921-river-based estimate, the discharge implied by the Fekete et al. runoff is lower for the Arctic and Atlantic Oceans and higher for the Pacific and Indian Oceans and the Mediterranean and Black Seas, whereas the ECMWF *P–E* implies higher discharge into all but the Pacific basin. Table 4 shows that both of the reanalysis *P–E* fields underestimate the discharge into the Pacific Ocean significantly—by 15% for ECMWF and 19% for NCEP compared with the river-based estimate. These biases result primarily from the smaller *P–E* than the Fekete et al. runoff over China and Southeast Asia (Fig. 2).

For the Arctic Ocean, estimates range from 2600 km^3 yr^{-1} by BR75 to 5220 km^3 yr^{-1} by Korzun et al. (1977). Grabs et al. (2000) obtained an annual discharge of 2603 km^3 into the Arctic Ocean by totaling discharge data from the 35 farthest downstream stations, which account for 70% of the total Arctic drainage area. Assuming the unmonitored 30% drainage area has similar runoff rates, this would imply a total discharge of 3718 km^3 yr^{-1}, which is comparable to our estimates (except for the NCEP case) (Table 4).

Figure 6 shows that the right amount of total discharge into a particular ocean basin may result from discharges coming off the wrong coasts. For example, the total discharge from the western and eastern coasts of the Indian Ocean is similar for the 921-river and

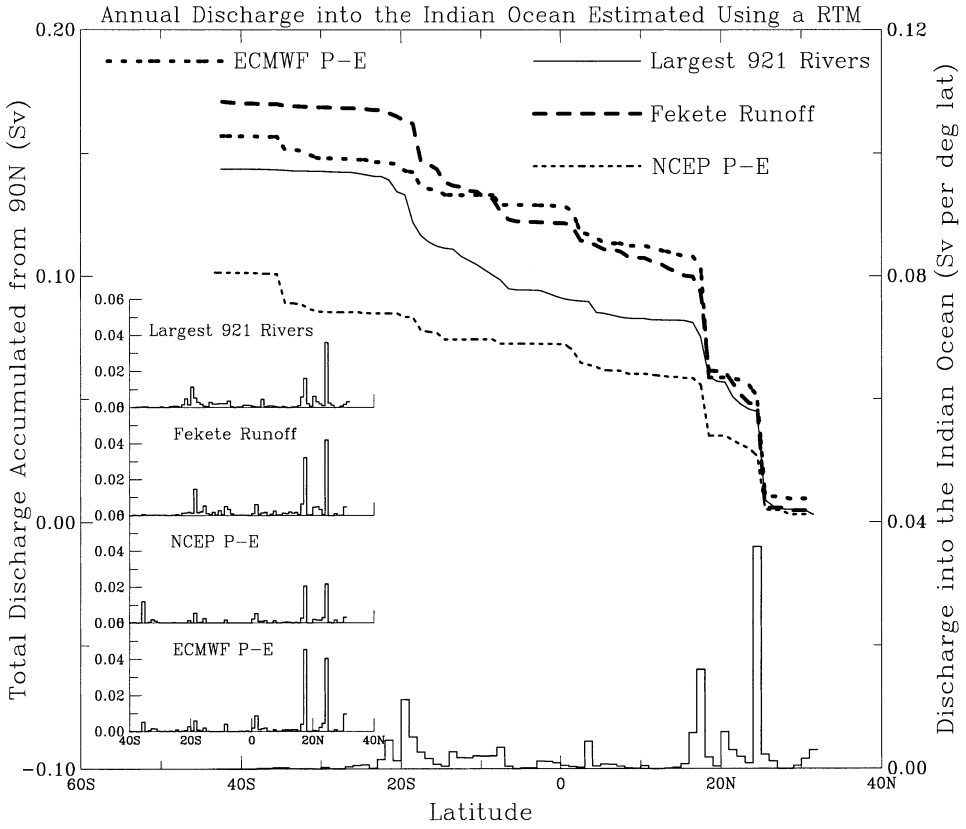

FIG. 10. Estimates of annual-mean continental freshwater discharge into the Indian Ocean for each 1° lat zone (right ordinate, lower stepwise lines and the inset) and the cumulated discharge starting from 90°N (upper curves).

NCEP cases, but the NCEP *P–E* implies too much runoff from Australia and too little from Africa.

b. Individual oceans

1) ATLANTIC OCEAN

The latitudinal distribution of the zonal and accumulated discharge into the Atlantic Ocean (Fig. 9) reveals that the Amazon accounts for more than one-third of the total discharge (~0.60 Sv). Other major rivers include the Congo, Orinoco, Mississippi, Paraná, and St. Lawrence (~0.011 Sv at 48.75°N). Most of the discharge comes from low-latitude America and Africa, although substantial freshwater fluxes also occur at 40°–60°N, mostly from North America. The Fekete et al. runoff and the two reanalysis *P–E* fields all slightly underestimate the river discharge at many latitudes within 15°–55°N. The NCEP *P–E* also underestimates the discharge from rivers between 3° and 7°N (such as no. 39 Sanaga) and from the Congo, which adds to its negative bias (≈−0.08 Sv for the total accumulated discharge). The ECMWF *P–E* overestimates discharge from the Orinoco River (by ~0.007 Sv), which compensates for the negative bias accumulated to the north, indicating a dislocation of the atmospheric moisture convergence. The ECMWF *P–E* also overestimates the discharge from the Congo by ~0.05 Sv. This approximately equals the overall bias in the ECMWF estimate of the accumulated discharge compared with the river-based estimate. In general, the discharge implied by the Fekete et al. runoff agrees well with the river-based estimate in the Atlantic basin.

2) INDIAN OCEAN

The zonal and accumulated discharge into the Indian Ocean (Fig. 10) reveals that the Brahmaputra/Ganges Rivers (0.033 Sv at 24.25°N) account for about one-quarter of the total discharge. Other large rivers entering the Indian Ocean include Irrawaddy (0.012 Sv at 17.75°N), Zambeze (0.0037 Sv at 18.25°S), Indus (0.0033 Sv at 24.00°N), Godavari (0.0031 Sv at 16.75°N), and Mahanadi (0.0023 Sv at 20.25°N). The Indian subcontinent and the coast of the Bay of Bengal provide the largest freshwater flux into the Indian Ocean around 15°–27°N. Substantial discharge also occurs on the eastern African coast between 6° and 24°S. There is little discharge from arid to semiarid western Australia.

The NCEP *P–E* underestimates the outflow from the

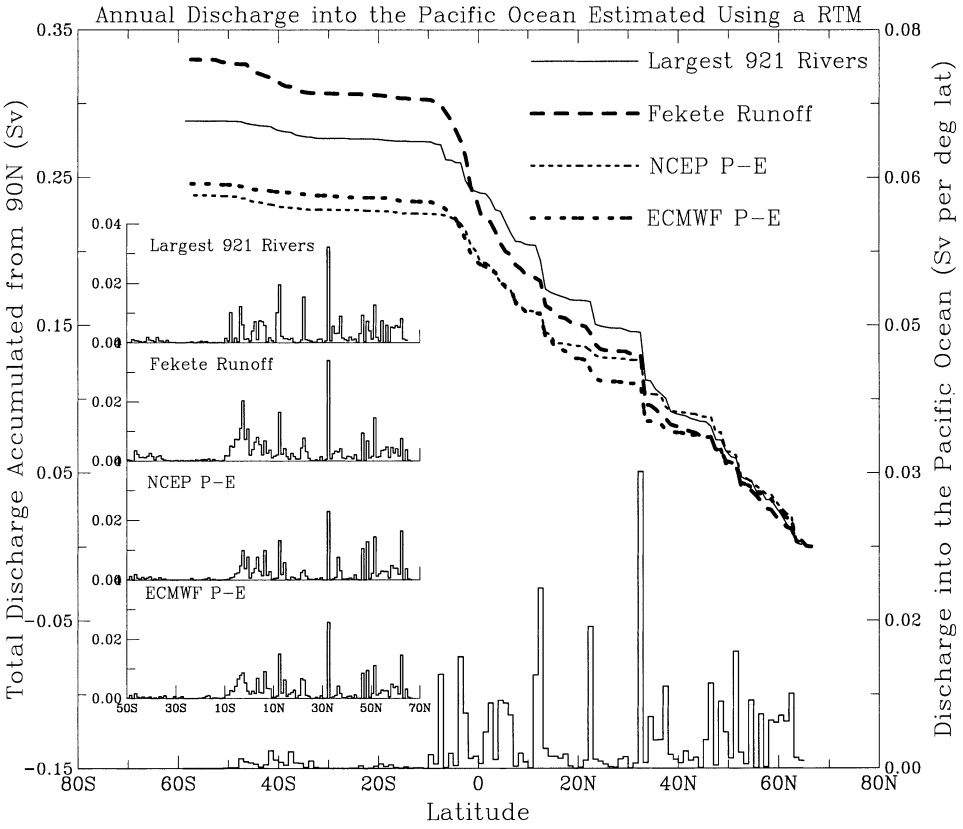

FIG. 11. Estimates of annual-mean continental freshwater discharge into the Pacific Ocean for each 1° lat zone (right ordinate, lower stepwise lines and the inset) and the cumulated discharge starting from 90°N (upper curves).

Brahmaputra/Ganges by ~37% and the Zambeze by ~50%, but overestimates discharge around 35°S (the latter bias is also seen in the ECMWF case). Hence, the NCEP-implied discharge into the Indian Ocean (~0.10 Sv) is substantially lower than the river-based estimate (~0.14 Sv). However, the ECMWF case overestimates outflow from the Irrawaddy by more than 100%, while the outflow from Zambeze is underestimated. While comparable with the river-based estimate at most latitudes, the discharge implied by the Fekete et al. runoff is also too high for the Irrawaddy.

3) PACIFIC OCEAN

The zonal and accumulated discharge into the Pacific Ocean (Fig. 11) features the Changjiang (~0.030 Sv at 32.25°N), Mekong (0.017 Sv around 12.0°N), Amur (0.011 Sv at 51.75°N), and Xijiang (0.0086 Sv at 22.25°N). The RTM underestimates the observed outflow from the Xijiang by over 50% when forced with the Fekete et al. runoff and the reanalysis *P–E* fields, while it puts higher outflows through nearby smaller rivers around 22.25°N. The outflow from the Changjiang is also underestimated in the NCEP (by 28%) and ECMWF (by 22%) cases. These negative biases are consistent with the negative *P–E* (set to zero in the RTM simulations) or smaller *P–E* values than the Fekete runoff over east Asia, the southwestern United States, and central America (Fig. 2).

Within 10°S–10°N, the RTM simulated discharge is more continuous than the river-based estimate, particularly for the Fekete et al. case, which results in a larger (by ~0.05 Sv) total accumulated discharge. The difference within 10°S–10°N results primarily from the Indonesia–Malaysia–New Guinea region, where a large number of class 3 and smaller rivers are not monitored (cf. Fig. 1), making our river-based estimate less reliable for this region. Further, the small islands and varying coastlines in this region are difficult to simulate accurately and require a resolution higher than 0.5°, as used by the RTM and the STN-30p river database. The latter was used in estimating the contribution by the unmonitored rivers in the river-based estimate. Therefore, substantial uncertainties on the order of 0.05 Sv exist for the discharge estimates from this region.

c. Seasonal variations

Figure 12 shows the mean annual cycle of total freshwater discharge into the individual and global oceans,

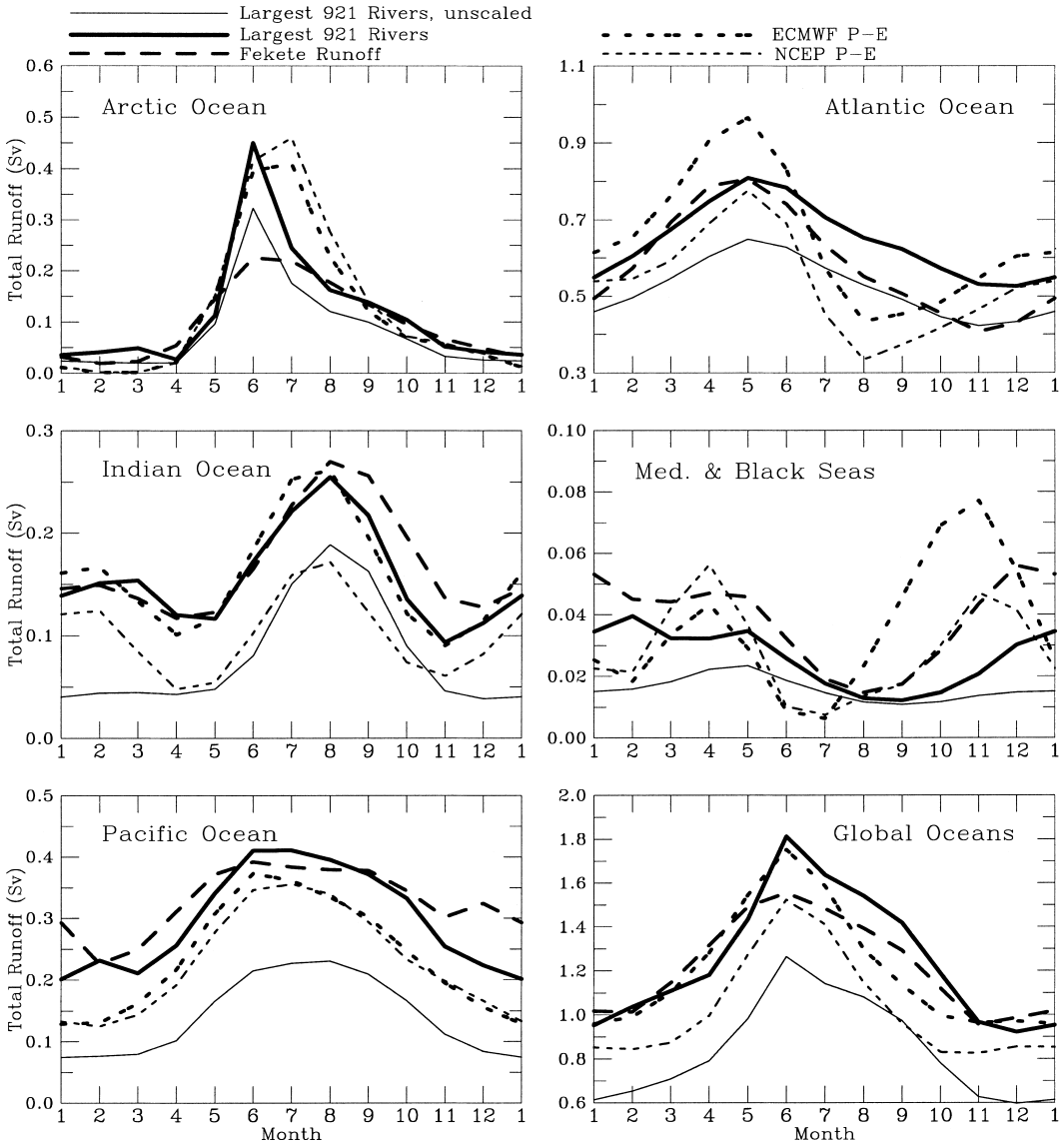

FIG. 12. Mean annual cycle of freshwater discharge into individual and global oceans based on various estimates. The thin, solid line is for the estimate based on the 921 rivers without scaling to account for the unmonitored areas.

as estimated based on the 921 rivers with and without scaling for the contribution from the unmonitored areas, Fekete et al. runoff, and *P–E* fields from the NCEP and ECMWF reanalyses. The inclusion of the unscaled gauge-based estimate shows that the contribution from the unmonitored areas does not significantly alter the phase of the mean annual cycle and is large, ranging from ~20% of the monitored discharge for the Atlantic to ~100% for the Pacific.

The discharge into the Arctic Ocean has a sharp peak in June arising from snowmelt in late spring, although the Fekete et al. result has a lower maximum but with higher values in most other months. Both the NCEP and ECMWF *P–E* fields result in too much discharge in July and too little from January to March. We tested various combinations of k and t_s (see section 3b) to account for snowmelt but all produced the peak discharge in July. This suggests that the simple scheme has limitations, probably arising from the use of only daily mean temperatures.

The total freshwater discharge into the Atlantic Ocean has a similar peak in May for all but the ECMWF and the unscaled cases (Fig. 12). For the Atlantic, the ECMWF case has too much discharge in May and too low discharge in August and September and the latter bias is even larger for the NCEP case. The May peak in all the cases results from the concurrence of high discharge in May from the Amazon and Mississippi (Fig. 5). The discharge into the Indian Ocean peaks in August, mainly from the heavy Indian summer monsoon

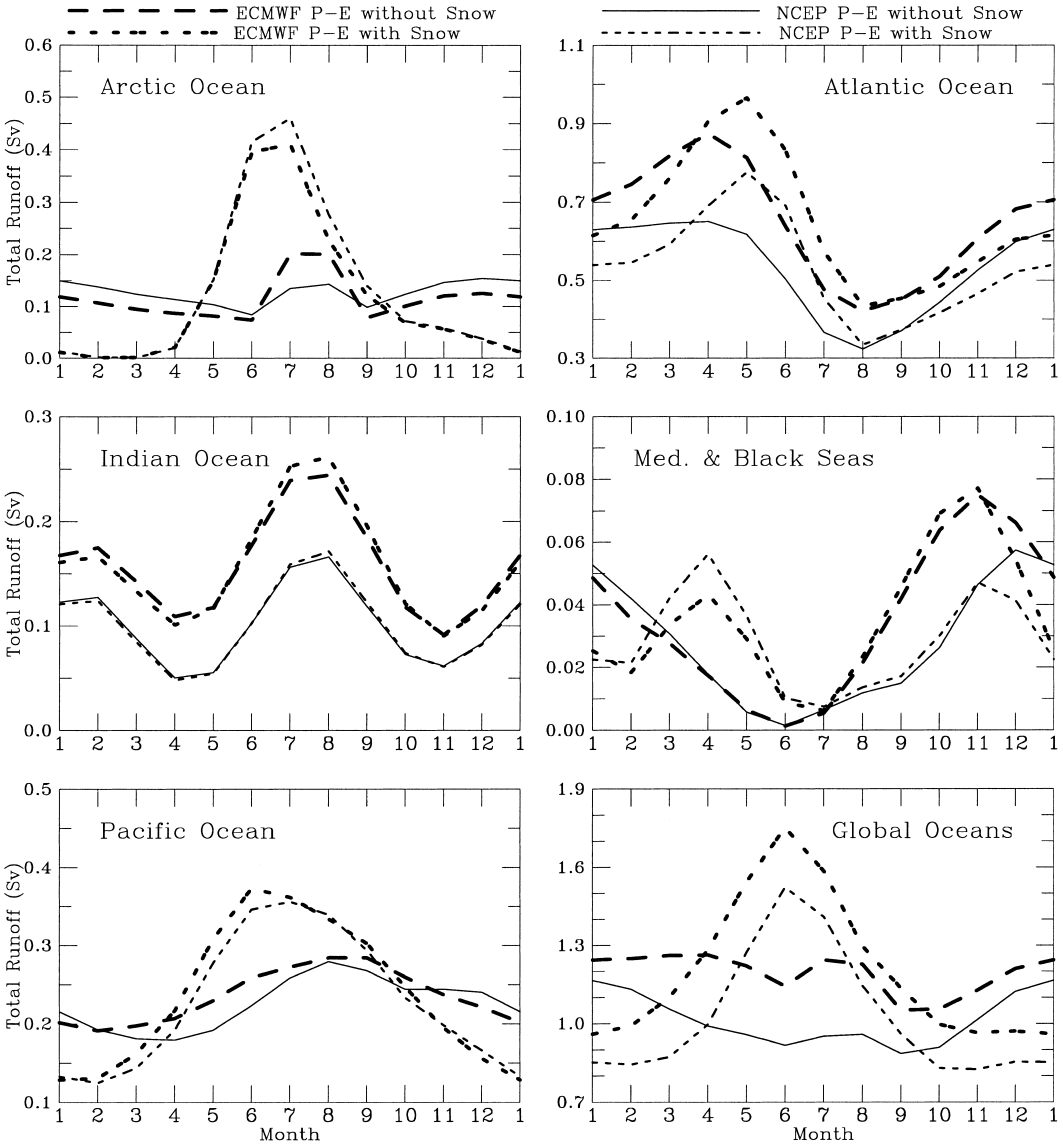

FIG. 13. Mean annual cycle of freshwater discharge into individual and global oceans estimated using ECMWF and NCEP *P–E* fields with and without the effects of snow.

rainfall. For the Pacific Ocean, the discharge peaks around June–July primarily because of heavy monsoon rainfall over east Asia during these months. Over the Mediterranean and Black Seas, the discharge is low in the warm season and high during the winter and spring seasons. Globally, total freshwater discharge is high from May to September with a peak in June and a lull from October to April. This annual cycle results mainly from the discharge from Northern Hemisphere land areas. All the cases broadly reproduce the annual cycles revealed by the gauge data.

Figure 13 shows the annual cycles estimated with and without the snow scheme (i.e., all *P–E* was considered as runoff) for the reanalysis *P–E* cases to illustrate the overall effects of snow accumulation and melt on continental discharge. It can be seen that without the snow effects, the discharge into the Arctic Ocean would be radically different and would not have the sharp June peak, the peak discharge into the Atlantic around May would also be considerably lower, the discharge into the Pacific would have a much lower peak in August instead of June, and the global discharge would have little seasonal variation. On the other hand, snow has negligible effects on the discharge into the Indian Ocean and Mediterranean and Black Seas.

7. Discussion

Our freshwater discharge estimates have various sources of errors. For example, the 921-river-based dis-

charge contains uncertainties associated with 1) the estimate of discharge from the unmonitored areas, 2) the adjustment for river mouth flow rates, 3) varying length and periods of streamflow records, and 4) varying human influences on the natural streamflow. We also did not include groundwater runoff and the runoff from Antarctica. For the reanalysis *P–E* fields, there are many documented regional biases such as those related to moisture convergence and the atmospheric circulation (Trenberth and Guillemot 1998; Trenberth et al. 2001a), as well as known problems in ERA-15 over Africa (e.g., the spurious ITCZ shift) and South America (Trenberth et al. 2001b). The Fekete et al. runoff has uncertainties arising from its use of limited streamflow data and a water balance model over many regions (Fekete et al. 2000). The strength of the Fekete et al. (2000) runoff is in its patterns of the distribution, but the calibration for the total amount contains uncertainties over many regions.

Nevertheless, we believe that the estimates based on the 921-river streamflow data, the Fekete et al. runoff, and the ECMWF *P–E* are likely to be close to the truth. In particular, we think the 921-river-based estimate is the most reliable, except perhaps for the Mediterranean and Black Seas where the estimate seems to be a bit too low (Table 4). This conclusion follows because the 921 rivers cover over two-thirds of world's actively drained land areas and the errors in computing the discharge from the unmonitored areas result primarily from the uncertainties in the Fekete et al. runoff through $r(j)$ in Eq. (2); that is, these errors are also in the Fekete et al. runoff-based estimate. The freshwater discharges implied by the reanalysis-derived *P–E* fields generally agree with the 921-river-based estimate, although large regional biases exist (cf. Fig. 2), especially for the NCEP *P–E*. This result suggests that the *P–E* products could be used as proxies of runoff over most land areas and, with some tuning and information about variability of groundwater, may be applied to study the interannual to decadal variations in continental freshwater discharge. The NCEP reanalysis is available for the last 50 years or so and an improved ECMWF reanalysis (ERA-40) for a similar period will soon become available. For such applications, however, improvements in accounting for the effects of snow accumulation and melt on seasonal to interannual timescales are needed. Furthermore, changes in human influences on the natural streamflow and evaporation over the last several decades will also be important considerations.

We have shown that comparisons of basinwide discharges (Table 4) have only limited value. It is obviously a more challenging task to derive correct estimates of discharge from all major rivers than just for the total discharge. For detailed evaluation of climate models and for estimating meridional transport of freshwater in the oceans, discharge from individual rivers (e.g., Table 2 and the appendix) and spatial distributions of discharge (Fig. 6) are needed. Because the freshwater fluxes from the large rivers are substantial, use of the unrealistic discharge distribution from BR75 in estimating oceanic meridional freshwater transport (e.g., Wijffels et al. 1992; Wijffels 2001) is likely to induce significant errors. Using the BR75 discharge for evaluating climate models (e.g., Pardaens et al. 2002) is also not a good choice.

8. Summary

We have created and compared several estimates of continental freshwater discharge into the oceans. The first is built on discharge data from 921 ocean-reaching rivers selected from several comprehensive streamflow datasets. The drainage area of the 921 rivers is 79.5×10^6 km^2, or about 68% of global non-ice, nondesert land areas. We estimated the river mouth outflow from the world's large rivers by adjusting the streamflow rate at the farthest downstream station using the ratio of simulated flow rates (or drainage areas in some cases) at the river mouth and the station. The discharge from the unmonitored areas was estimated based on the ratios of runoff and drainage area between the unmonitored and monitored areas at each latitude. A river transport model, the composite runoff field from Fekete et al. (2000), and a simulated global river database, STN-30p, were used in this analysis. Long-term mean annual and monthly freshwater discharge at each latitude into individual and global oceans were derived based on the adjusted river outflow and the estimated contribution from unmonitored areas.

Second, we have separately computed annual and monthly continental discharge at each latitude into the oceans by forcing the RTM with the Fekete et al. runoff and the *P–E* fields derived from the NCEP and ECMWF reanalyses with a adjustment for snow effects. These implied discharges were compared with that derived from the streamflow data. The main results are summarized as follows.

1) The use of river mouth outflow increases the global continental discharge by ~18.7% and the total drainage area by ~20.4% compared with estimates using the unadjusted data from the farthest downstream stations (cf. Fig. 1). This result suggests that using unadjusted streamflow data from the farthest downstream stations (e.g., Perry et al. 1996; Grabs et al. 1996, 2000) substantially underestimates global continental freshwater discharge.
2) Globally, the annual runoff rate over the unmonitored areas is comparable to that over the monitored areas, although their ratio varies from 0.29 for the Indian Ocean drainage basin in July to 4.30 for the Pacific Ocean drainage basin in January (Table 3).
3) Our 921-river-based estimate of global continental

freshwater discharge (excluding Antarctica[3]) is 37 288 ± 662 km^3 yr^{-1}, or 1.18 ± 0.02 Sv, which is ~7.6% of global *P* and 35% of terrestrial *P*. Although this value is comparable to earlier estimates, large differences exist among the discharges into the individual ocean basins. The estimates of global discharge based on the Fekete et al. runoff and ECMWF *P–E* are slightly higher than the river-based estimate, while the NCEP *P–E* implies lower discharge (Table 4). In general, the reanalysis *P–E* fields underestimate discharge from east Asia and northern Africa (Fig. 6). About 57% of the global discharge comes from the world's 50 largest rivers (Table 2).

4) When forced with the Fekete et al. runoff and reanalysis *P–E* fields, the RTM simulates the station streamflow rates reasonably well for world's major rivers (Figs. 3, 4, and 6). This is especially true for the Fekete et al. runoff case (Table 2 and the appendix) and suggests that river transport models at 0.5° resolution, such as the one used in the NCAR CCSM, can realistically simulate the world river system and its routing of terrestrial runoff into the oceans.
5) The continental discharges into the oceans within each 1° latitude band implied by the Fekete et al. runoff and reanalysis *P–E* fields agree reasonably well with the river-based estimates, which we regard as the closest to the truth. This is particularly true for the Fekete et al. runoff and ECMWF *P–E* cases and for the global oceans and the Atlantic Ocean (Figs. 7 and 9). In general, the NCEP *P–E* underestimates continental discharge at many latitudes for all the ocean basins except for the Arctic Ocean.
6) The latitudinal distribution of accumulative discharge into the global oceans estimated based on the 921 rivers is similar to that from BR75, although the discharge at individual latitudes differs greatly. The BR75 estimate is unrealistically smooth (Figs. 7 and 8) even compared with our 5° smoothed discharge. Our continental discharge has realistic latitudinal distributions that are needed for reliable estimates of meridional transport of freshwater in the oceans. Earlier estimates (e.g., Wijffels et al. 1992; Wijffels 2001) may contain significant errors as a result of using the unrealistic latitudinal distribution of continental discharge from BR75.
7) Discharges from most of the world's largest rivers have large annual cycles. For example, the Amazon peaks in May–June, Orinoco peaks in August, Changjiang peaks around July; whereas large Russian rivers (e.g., Yenisey, Lena, Ob,) have a sharp peak in June arising from snowmelt (Fig. 5). Basinwide-integrated precipitation usually does not have the same seasonal phase as for river discharge, which illustrates the important effects of snow accumulation and melt and river transport. The total discharge into the Arctic, the Pacific, and the global oceans peaks in June, whereas the peak is in May for the Atlantic Ocean and in August for the Indian Ocean (Fig. 12). Snow accumulation and melt have large effects on the annual cycle of discharge into the Arctic, Atlantic, Pacific, and global oceans, but little influence on the discharge into the Indian Ocean and the Mediterranean and Black Seas.

The long-term mean values of river runoff and continental discharge reported here is available for free download from NCAR's Climate Analysis Section catalog (http://www.cgd.ucar.edu/cas/catalog/).

Acknowledgments. We thank W. G. Large and G. B. Bonan for helpful discussions, S. Sorooshian, D. P. Lettenmaier, and two reviewers for helpful comments, S. Levis for help with the RTM codes, M. L. Branstetter and J. S. Famiglietti for providing the RTM, J. Caron for help with the reanalysis datasets, and B. M. Fekete, C. J. Vörösmarty, B. A. Bodo, and others for making the streamflow, runoff, and STN-30p datasets available. This research was sponsored by grants from NOAA's Office of Global Programs and jointly by NOAA–NASA under NOAA Grant NA17GP1376.

[3] Jacobs et al. (1992) gave a total freshwater flux of 2613 km^3 yr^{-1} from Antarctica into the ocean, of which 2016 km^3 yr^{-1} is from icebergs, 544 km^3 yr^{-1} from ice shelf melting, and 53 km^3 yr^{-1} from surface and underground runoff.

REFERENCES

Adler, R. F., C. Kidd, G. Petty, M. Morissey, and H. M. Goodman, 2001: Intercomparison of global precipitation products: The third Precipitation Intercomparison Project (PIP-3). *Bull. Amer. Meteor. Soc.*, **82,** 1377–1396.

Baumgartner, A., and E. Reichel, 1975: *The World Water Balance.* Elsevier, 179 pp.

Blackmon, M., and Coauthors, 2001: The Community Climate System Model. *Bull. Amer. Meteor. Soc.*, **82,** 2357–2376.

Bodo, B. A., 2001: Annotations for monthly discharge data for world rivers (excluding former Soviet Union). NCAR, 85 pp. [Available online at http://dss.ucar.edu/datasets/ds552.1/docs/.]

Branstetter, M. L., 2001: Development of a parallel river transport algorithm and applications to climate studies. Ph.D. dissertation, University of Texas at Austin, 119 pp.

——, and J. S. Famiglietti, 1999: Testing the sensitivity of GCM-simulated runoff to climate model resolution using a parallel river transport algorithm. Preprints, *14th Conf. on Hydrology,* Dallas, TX, Amer. Meteor. Soc., 391–392.

Carton, J. A., 1991: Effect of the surface freshwater flux on sea surface temperature in the tropical Atlantic Ocean. *J. Geophys. Res.*, **96,** 12 593–12 598.

Church, J. A., and Coauthors, 2001: Changes in sea level. *Climate Change 2001: The Scientific Basis,* J. T. Houghton et al., Eds., Cambridge University Press, 639–694.

Dai, A., and I. Fung, 1993: Can climate variability contribute to the "missing" CO_2 sink? *Global Biogeochem. Cycles,* **7,** 599–609.

——, G. A. Meehl, W. M. Washington, T. M. L. Wigley, and J. A. Arblaster, 2001a: Ensemble simulation of twenty-first century climate changes: Business-as-usual versus CO_2 stabilization. *Bull. Amer. Meteor. Soc.*, **82,** 2377–2388.

——, T. M. L. Wigley, G. A. Meehl, and W. M. Washington, 2001b: Effects of stabilizing atmospheric CO_2 on global climate in the next two centuries. *Geophys. Res. Lett.*, **28,** 4511–4514.

Daly, C., R. P. Neilson, and D. L. Phillips, 1994: A statistical–topographical model for mapping climatological precipitation over mountainous terrain. *J. Appl. Meteor.,* **33,** 140–158.

Dümenil, L., K. Isele, H.-J. Liebscher, U. Schröder, M. Schumacher, and K. Wilke, 1993: Discharge data from 50 selected rivers for GCM validation. Rep. 100, Max Planck Institute and Global Runoff Data Centre, Hamburg, Germany, 61 pp.

Fekete, B. M., C. J. Vörösmarty, and W. Grabs, 2000: Global composite runoff fields based on observed river discharge and simulated water balances. Global Runoff Data Centre Rep. 22, Koblenz, Germany, 39 pp. plus annex. [Available online at http://www.bafg.de/grdc.htm.]

——, ——, and ——, 2002: High resolution fields of global runoff combining observed river discharge and simulated water balances. *Global Biogeochem. Cycles,* **16,** doi: 10.1029/1999GB001254.

Gibson, J. K., P. Kallberg, S. Uppala, A. Hernandez, A. Nomura, and E. Serrano, 1997: ERA description. ECMWF Reanalysis Project Rep. 1, 72 pp.

Grabs, W. E., T. de Couet, and J. Pauler, 1996: Freshwater fluxes from continents into the world oceans based on data of the global runoff data base. Global Runoff Data Centre Rep. 10, Koblenz, Germany, 228 pp. [Available from GRDC, Federal Institute of Hydrology, Kaiserin-Augusta-Anlagen 15-17, D-56068 Koblenz, Germany.]

——, F. Portmann, and T. de Couet, 2000: Discharge observation networks in Arctic regions: Computation of the river runoff into the Arctic Ocean: Its seasonality and variability. *The Freshwater Budget of the Arctic Ocean,* E. L. Lewis, et al., Eds., Kluwer Academic, 249–267.

Hagemann, S., and L. D. Gates, 2001: Validation of the hydrological cycle of ECMWF and NCEP reanalyses using the MPI hydrological discharge model. *J. Geophys. Res.,* **106,** 1503–1510.

Haxeltine, A., and I. C. Prentice, 1996: BIOME3: An equilibrium terrestrial biosphere model based on ecophysiological constraints, resource availability, and competition among plant functional types. *Global Biogeochem. Cycles,* **10,** 693–709.

Huffman, G. J., and Coauthors, 1997: The Global Precipitation Climatology Project (GPCP) combined precipitation data set. *Bull. Amer. Meteor. Soc.,* **78,** 5–20.

Jacobs, S. S., H. Hellmer, C. Doake, and R. Frolich, 1992: Melting of ice shelves and the mass balance of Antarctica. *J. Glaciol.,* **38,** 375–387.

Kalnay, E., and Coauthors, 1996: The NCEP/NCAR 40-Year Reanalysis Project. *Bull. Amer. Meteor. Soc.,* **77,** 437–471.

Korzun, V. I., A. A. Sokolov, M. I. Budyko, K. P. Voskrensensky, G. P. Kalinin, A. A. Konoplyantsev, E. S. Korotkevich, and M. I. Lvovich, 1977: *Atlas of the World Water Balance.* UNESCO, 36 pp. plus 65 maps.

Lvovich, M. I., 1970: World water balance (general report). *World Water Balance: Proceedings of the Reading Symposium,* IASH–UNESCO–WMO Publ. 93, 401–415.

Marcinek, J., 1964: The river discharge from land surface over the globe and its distribution in 5° zones (in German). *Bulletin of the Institute of Water Management,* Vol. 21, 204 pp.

Maurer, E. P., B. Nijssen, and D. P. Lettenmaier, 2000: Use of reanalysis land surface water budget variables in hydrologic studies. *GEWEX News,* Vol. 10, No. 4, 6–8.

Miller, J. R., G. L. Russell, and G. Caliri, 1994: Continental-scale river flow in climate models. *J. Climate,* **7,** 914–928.

Milly, P. C. D., and K. A. Dunne, 2001: Trends in evaporation and surface cooling in the Mississippi River basin. *Geophys. Res. Lett.,* **28,** 1219–1222.

Nakamura, M., 1996: Effects of ice albedo and runoff feedbacks on the thermohaline circulation. *J. Climate,* **9,** 1783–1794.

New, M., M. Hulme, and P. Jones, 1999: Representing twentieth-century space–time climate variability. Part I: Development of a 1961–90 mean monthly terrestrial climatology. *J. Climate,* **12,** 829–856.

Nijssen, B., G. M. O'Donnell, D. P. Lettenmaier, D. Lohmann, and E. F. Wood, 2001: Predicting discharge of global rivers. *J. Climate,* **14,** 3307–3323.

Oki, T., 1999: The global water cycle. *Global Energy and Water Cycles,* K. A. Browning and R. J. Gurney, Eds., Cambridge University Press, 10–29.

Pardaens, A. K., H. T. Banks, J. M. Gregory, and P. R. Rowntree, 2002: Freshwater transport in HadCM3. *Climate Dyn.,* in press.

Perry, G. D., P. B. Duffy, and N. L. Miller, 1996: An extended data set of river discharges for validation of general circulation models. *J. Geophys. Res.,* **101,** 21 339–21 349.

Probst, J. L., and Y. Tardy, 1987: Long-range streamflow and world continental runoff fluctuations since the begining of this century. *J. Hydrol.,* **94,** 289–311.

Shiklomanov, A. I., R. B. Lammers, and C. J. Vörösmarty, 2002: Widespread decline in hydrological monitoring threatens pan-Arctic research. *Eos, Trans. Amer. Geophys. Union,* **83,** 13–16.

Stendel, M., and K. Arpe, 1997: Evaluation of the hydrological cycle in reanalyses and observations. Max-Planck-Institut für Meteorologie Rep. 228, 52 pp.

Trenberth, K. E., and C. J. Guillemot, 1996: Evaluation of the atmospheric moisture and hydrological cycle in the NCEP reanalyses. NCAR Tech. Note NCAR/TN-430+STR, 300 pp.

——, and ——, 1998: Evaluation of the atmospheric moisture and hydrological cycle in the NCEP/NCAR reanalyses. *Climate Dyn.,* **14,** 213–231.

——, J. M. Caron, and D. P. Stepaniak, 2001a: The atmospheric energy budget and implications for surface fluxes and ocean heat transports. *Climate Dyn.,* **17,** 259–276.

——, D. P. Stepaniak, J. W. Hurrell, and M. Fiorino, 2001b: Quality of reanalyses in the Tropics. *J. Climate,* **14,** 1499–1510.

Vörösmarty, C. J., B. M. Fekete, M. Meybeck, and R. B. Lammers, 2000: Global system of rivers: Its role in organizing continental land mass and defining land-to-ocean linkages. *Global Biogeochem. Cycles,* **14,** 599–621.

Wijffels, S. E., 2001: Ocean transport of fresh water. *Ocean Circulation and Climate,* G. Siedler, J. Church, and J. Gould, Eds., Academic Press, 475–488.

——, R. W. Schmitt, H. L. Bryden, and A. Stigebrandt, 1992: Transport of freshwater by the oceans. *J. Phys. Oceanogr.,* **22,** 155–162.

Xie, P., and P. A. Arkin, 1997: Global precipitation: A 17-year monthly analysis based on gauge observations, satellite estimates, and numerical model outputs. *Bull. Amer. Meteor. Soc.,* **78,** 2539–2558.

Yang, D., and Coauthors, 2001: Compatibility evaluation of national precipitation gage measurements. *J. Geophys. Res.,* **106,** 1481–1491.

APPENDIX

Flow Rates and Drainage Areas of World's Largest Rivers.

World's largest 150 rivers (by the estimated river mouth flow rate, Vol), plus 50 rivers that are among the top 150 rivers by drainage area but do not meet the volume criterion. Listed are long-term mean station (Stn ± std dev) and river transport model (RTM) simulated river flow (in $km^3\ yr^{-1}$) at the station location, and the estimated annual volume (Vol) and drainage area (DA), based on STN-30p, in $10^3\ km^2$) at the river mouth. The composite annual runoff data of Fekete et al. (2000) were used in the RTM simulation. Nyr is station record length in yr, lon and lat are longitude and latitude for the station.

No.	Name	Vol at station		River mouth		Stn DA	Nyr	Lon (°)	Lat (°)	Station, country
		Stn ± std dev	RTM	Vol	DA					
Total of top 50 rivers from Table 2:										
		17 492 ± 552	18 079	21 152	50 415	42 364				
51	San Juan	65 ± 8	21	65	18	14	26	−77.2	4.2	Penitas, Colombia
52	Bénoué	12 ± 3	3	64	339	61	38	13.4	9.3	Garoua-dono, Cameroon
53	Kuskokwim	38 ± 7	1	57	116	81	47	−158.1	61.9	Crooked Creek, AK, United States
54	Albany	30 ± 9	25	57	133	118	28	−83.9	51.3	Near Hat Isla, Canada
55	Huai	27 ± 15	17	57	244	121	54	117.4	32.9	Bengbu, China
56	La Grande	54 ± 8	69	56	99	96	19	−78.6	53.7	en aval de, Canada
57	Tigris	38 ± 12	37	56	221	134	34	44.4	33.3	Baghdad, Iraq
58	Krishna	52 ± 17	86	55	252	251	74	80.6	16.5	Vijayawada, India
59	Ottawa	37 ± 8	18	55	133	90	72	−76.2	45.5	Chats Falls, Canada
60	Chindwin	77 ± 12	69	55	124	27	11	95.7	26.0	Hkamti, Myanmar (Burma)
61	Taz	33 ± 5	61	55	129	100	28	82.3	66.6	Sidorovsk, Russia
62	Po	48 ± 12	66	55	102	70	80	11.6	44.9	Pontelagosc, Italy
63	Courantyne	34 ± 9	10	54	68	52	7	−57.7	5.0	Mataway (Suriname)
64	Indigirka	50 ± 10	51	54	324	305	58	147.5	69.6	Vorontsovo, Russia
65	Rhone	54 ± 11	39	54	99	96	80	4.6	43.8	Beaucaire, France
66	Saguenay	46 ± 6	50	53	86	73	70	−71.6	48.6	Centrale d', Canada
67	Alabama	29 ± 7	25	51	124	57	46	−87.5	31.5	Claiborne, AL, United States
68	Stikine	51 ± 6	21	51	51	52	21	−132.1	56.7	Near Wrangell, AK, United States
69	Eastmain	29 ± 4	32	49	43	44	21	−78.1	52.2	tete de la, Canada
70	Brahmani	21	7	48	57	50	1	85.0	21.5	Barakot bri, India
71	Dnepr	47 ± 13	108	47	509	463	33	35.2	47.9	Dnepr hydro, Ukraine
72	Huanghe	45 ± 14	60	47	894	734	31	114.9	35.2	Gaocung, China
73	Jamanxim	37 ± 8	22	47	58	40	3	−55.8	−5.5	Jamanxim, Brazil
74	Susquehanna	31 ± 7	26	46	72	62	109	−76.9	40.2	Harrisburg, PA, United States
75	Beijiang	42 ± 11	22	46	34	38	33	112.9	23.6	Shijiao, China
76	Don	26 ± 10	24	45	423	378	101	40.7	47.5	Razdorskaya, Russia
77	Susitna	45 ± 5	25	45	46	50	19	−150.5	6.5	Susitna Station, AK, United States
78	Narmada	39 ± 14	11	44	114	89	26	73.7	21.9	Garudeshwar, India
79	Santa Cruz	22 ± 3	11	41	26	16	38	−71.9	−50.3	Charles Fuh, Argentina
80	Oyapock	28 ± 5	29	40	31	25	7	−51.9	3.8	Maripa, French Guiana
81	George	24 ± 3	15	40	39	35	16	−65.8	58.2	aux Chutes, Canada
82	Rufiji	26 ± 8	27	40	187	158	17	37.9	−7.8	Stiegeler's, Tanzania
83	Nile	40 ± 2	309	40	3826	2900	12	31.3	29.7	El Ekhsase, Egypt
84	Nottaway	33 ± 5	26	39	74	58	22	−77.4	50.1	tete du Lac, Canada
85	Volta	34 ± 18	46	37	398	394	47	0.1	6.2	Senchi (Hal, Ghana)
86	Willamette	21 ± 5	20	37	31	19	84	−123.0	44.9	Salem, OR, United States
87	Skeena	29 ± 4	13	36	58	42	51	−128.4	54.6	Usk, Canada
88	Garonne	19 ± 6	19	36	58	52	58	0.2	44.4	Mas-d'Agena, France
89	Red	28 ± 12	34	36	219	175	55	−92.4	31.3	Alexandria, LA, United States

APPENDIX

Flow Rates and Drainage Areas of World's Largest Rivers.

(*Continued*)

No.	Name	Vol at station		River mouth		Stn DA	Nyr	Lon (°)	Lat (°)	Station, country
		Stn ± std dev	RTM	Vol	DA					
90	Pahang	18 ± 7	22	35	34	19	21	102.4	3.4	Temerloh, Malaysia
91	Moose	25 ± 5	21	34	115	61	23	−81.3	50.8	Moose River, Canada
92	Chao Phraya	29 ± 7	21	34	142	119	44	100.1	15.3	Wat Phikun, Thailand
93	Cuyuni	34 ± 10	25	34	49	53	5	−58.8	6.4	Kamaria Fal, Guyana
94	Vistula	33 ± 7	53	34	181	194	87	18.8	54.1	Tczew, Poland
95	Copper	34 ± 4	13	34	67	53	36	−144.5	61.5	Chitina, AK, United States
96	Saint John	27 ± 5	17	34	53	40	18	−66.8	46.0	d/s Mactaqu, Canada
97	Olenek	32 ± 7	41	34	212	198	24	123.7	71.9	7.5 km d/s, Russia
98	Rupert	27 ± 3	26	33	58	41	30	−76.9	51.5	en aval du, Canada
99	Vuoksi	19 ± 4	16	33	106	61	138	28.8	61.2	Tainionkosk, Finland
100	Kamchatka	29 ± 3	50	33	51	52	47	161.6	56.3	Bolshie Sch, Russia
101	Manicouagan	29 ± 6	30	33	46	46	25	−68.3	49.2	Centrale Mc, Canada
102	Esmeraldas	27 ± 5	16	32	19	19	5	−79.4	0.5	d.j. Sade, Ecuador
103	Doce	32 ± 9	33	32	90	78	25	−40.1	−19.4	Linhares, Brazil
104	Yana	32 ± 9	22	32	235	224	23	136.1	70.8	Ubileynaya, Russia
105	Jari	32 ± 10	12	32	46	51	31	−52.6	−0.6	Sao Francis, Brazil
106	Bío Bío	32 ± 10	35	32	20	24	28	−73.1	−36.8	Desembocadu, Chile
107	Severn	20 ± 6	21	32	104	94	21	−88.3	55.4	Limestone R, Canada
108	Nushagak	21 ± 3	19	31	35	26	11	−157.5	59.3	Ekwok, AK, United States
109	Tsiribihina	31 ± 10	34	31	49	45	24	45.0	−19.7	Betomba, Madagascar
110	Baker	27 ± 3	6	30	23	24	22	−72.9	−47.3	La Colonia, Chile
111	Araguari	30 ± 7	21	30	43	23	34	−51.4	0.7	Porto Plato, Brazil
112	Pur	28 ± 3	100	29	92	95	48	78.2	67.0	Samburg, Russia
113	Nass	25 ± 2	18	29	24	19	45	−129.1	55.2	u/s Shumal, Canada
114	Douro	17 ± 9	19	29	97	91	37	−7.8	41.2	Regua, Portugal
115	Negro	27 ± 7	8	29	198	95	67	−63.7	−40.5	Primera Ang, Argentina
116	Kouilou	29 ± 5	25	29	62	55	23	12.1	−4.1	Sounda, Congo
117	Loire	26 ± 9	10	28	118	110	116	−0.8	47.4	Montjean, France
118	Puelo	21 ± 3	21	28	11	9	43	−72.2	−41.5	Carrero de, Chile
119	Dongjiang	23 ± 6	33	27	34	25	29	114.3	23.2	Boluo, China
120	Tista	27 ± 5	12	27	19	20	6	89.5	25.8	Kaunia, Bangladesh
121	Elbe	22 ± 6	23	27	149	124	69	11.8	53.0	Wittenberge, Germany
122	Alsek	27 ± 4	8	27	26	28	8	−138.1	59.4	Near Yakutat, AK, United States
123	Tombigbee	21 ± 6	23	27	62	40	67	−87.9	32.5	Demopolis Lake, AL, United States
124	Paraiba do S	26 ± 8	7	26	63	56	71	−41.3	−21.8	Campos-Pont, Brazil
125	Parnaiba	24 ± 8	29	26	331	282	35	−42.4	−3.5	Porto Formo, Brazil
126	Karun	24 ± 8	27	25	63	61	72	48.7	31.3	Ahvaz, Iran
127	Curua-2	27 ± 5	24	25	31	35	21	−54.5	−5.6	Cajueiro, Brazil
128	Mezen	20 ± 3	8	25	65	56	73	45.6	65.0	Malonisogor, Russia
129	Kinabatangan	18 ± 2	10	25	12	11	3	117.6	5.3	Balat, Malaysia

APPENDIX

Flow Rates and Drainage Areas of World's Largest Rivers.

(*Continued*)

No.	Name	Vol at station		River mouth		Stn DA	Nyr	Lon (°)	Lat (°)	Station, country
		Stn ± std dev	RTM	Vol	DA					
130	Saint-Maurice	24 ± 6	61	24	38	42	84	−72.7	46.6	Centrale de, Canada
131	Nyanga	16 ± 3	15	23	25	20	6	10.7	−2.7	Ibanga, Gabon
132	Capim	18 ± 6	11	23	46	38	27	−47.8	−2.5	Badajos, Brazil
133	Grijalva	17 ± 3	6	22	50	38	33	−93.2	18.0	Reforma, Mexico
134	Senegal	22 ± 5	56	22	847	268	65	−15.5	16.5	Dagana, Senegal
135	Papaloapan	22 ± 5	22	22	26	21	32	−96.1	18.2	Papaloapan, Mexico
136	Euphrates	19 ± 7	37	21	221	274	18	44.3	32.7	Hindiya, Iraq
137	Glomma	21 ± 3	19	21	43	40	83	11.1	59.6	Langnes (So, Norway)
138	Apalachicola	20 ± 6	3	20	55	45	71	−84.9	30.7	Chattahoochee, FL, United States
139	Nadym	15 ± 3	14	20	53	48	35	72.7	65.6	Nadym, Russia
140	Odra	17 ± 4	10	20	120	110	87	14.3	52.8	Gozdowice, Poland
141	Daugava	16 ± 4	12	19	83	70	59	25.9	56.5	Jekabpils, Latvia
142	Hayes, MB	19 ± 4	10	19	94	103	18	−92.8	56.4	d/s Gods Ri, Canada
143	Baleine	17 ± 4	6	19	46	36	33	−77.0	55.2	Baleine GR, Canada
144	Mangoky	19 ± 6	9	19	60	53	13	43.9	−21.8	Bevoay, Madagascar
145	Feuilles	19 ± 2	22	19	46	42	25	−70.4	58.6	en aval de, Canada
146	Melezes	19 ± 3	11	19	51	43	30	−69.6	57.7	pres de la, Canada
147	Churchill	18 ± 5	11	18	316	287	22	−94.6	58.1	Churchill River, Canada
148	Kelantan	18 ± 4	21	18	6	12	39	102.2	5.8	Guillemard, Malaysia
149	Clutha	17 ± 4	14	17	15	20	29	169.7	−46.2	Balclutha, New Zealand
150	Cross	17 ± 3	12	17	12	7	13	9.3	5.8	Mamfe (Manf), Cameroon
151	Kemi	17 ± 3	26	17	50	51	74	24.7	65.9	Taivalkoski, Finland
152	Göta	17 ± 3	12	17	51	47	178	12.4	58.4	Vänern, Sweden
153	Han	17 ± 5	14	17	20	25	25	127.0	37.5	Indogyo, South Korea
154	Back	16 ± 3	1	17	106	94	29	−96.5	66.1	u/s Hermann, Canada
155	Onega	16 ± 3	6	16	59	56	51	38.5	63.8	Porog, Russia
156	Tapi	16 ± 7	4	16	66	62	27	72.9	21.3	Kathore, India
157	Anabar	13 ± 3	5	16	94	79	35	114.1	72.0	Saskylakh, Russia
158	Jequitinhonh	14 ± 5	16	14	68	68	55	−39.5	−15.9	Itapebi, Brazil
159	Kuban	11 ± 2	12	14	64	48	56	38.2	45.2	Tikhovskiy, Russia
160	Pánuco	14 ± 5	16	14	92	58	23	−98.6	22.0	Las Adjunta, Mexico
161	Limpopo	12 ± 4	15	14	420	342	3	33.0	−24.5	Chokwe, Mozambique
162	Winisk	13 ± 5	8	13	62	50	26	−87.2	54.5	Downstream Ashewei, Canada
163	Ebro	13 ± 4	26	13	83	84	23	0.5	40.8	Tortosa, Spain
164	Narva	12 ± 3	13	12	58	56	80	28.2	59.4	Narva Ges, Estonia
165	Colorado	11 ± 9	13	12	808	629	72	−114.6	32.7	Yuma, AZ, United States
166	Seine	11 ± 2	2	11	73	65	7	1.2	49.3	Poses, France
167	Coopermine	11 ± 3	1	11	49	51	4	−115.4	67.7	Coppermine, Canada
168	Dnestr	10 ± 3	18	11	72	66	76	29.5	46.8	Bendery, Moldova
169	Tagus	11 ± 6	12	11	73	67	16	−8.4	39.5	Almourol, Portugal
170	Burdekin	10 ± 10	8	10	121	129	47	147.2	−19.8	Clare, Australia

APPENDIX

Flow Rates and Drainage Areas of World's Largest Rivers.

(*Continued*)

No.	Name	Vol at station		River mouth		Stn DA	Nyr	Lon (°)	Lat (°)	Station, country
		Stn ± std dev	RTM	Vol	DA					
171	Itapecuru	7.4 ± 4.3	5.5	9.9	74	51	30	−44.4	−3.6	Cantanhede, Brazil
172	Murray	8.5 ± 7.3	15.2	9.4	1032	991	70	142.8	−34.6	Euston weir, Australia
173	Bolshoy Anyu	8.3 ± 1.9	14.7	8.4	50	50	11	161.2	68.2	Konstantino, Russia
174	Grande de Sa	8.4 ± 3.2	7.9	8.4	192	129	26	−105.1	21.8	El Capomal, Mexico
175	Bandama	8.3 ± 5.0	4.8	8.3	104	96	38	−4.8	5.9	Tiassalé, Ivory Coast
176	Cauvery	7.7 ± 2.7	4.5	7.7	79	74	5	78.8	10.8	Grand Anicu, India
177	Juba	6.1 ± 1.6	11.5	7.5	234	180	26	42.5	3.8	Luug (Lugh), Somalia
178	Fitzroy-QX	7.4 ± 4.8	5.2	7.4	138	136	10	150.1	−23.1	The Gap, Australia
179	Brazos	6.7 ± 3.9	5.2	7.1	125	117	81	−95.8	29.6	Richmond, TX, United States
180	Comoé	6.0 ± 3.6	3.4	6.8	82	67	39	−3.7	6.6	Aniassué, Ivory Coast
181	Jaguaribe	3.7 ± 4.1	3.5	6.6	77	48	21	−38.2	−5.2	Peixe Gordo, Brazil
182	Daly	6.3 ± 3.0	7.1	6.3	54	47	8	130.7	−13.8	Mount Nancar, Australia
183	Ouémé	5.4 ± 3.1	1.1	5.4	52	47	32	2.5	6.9	Bonou, Benin
184	Guadiana	4.8 ± 4.1	0.7	5.2	65	61	44	−7.6	37.8	Pulo do Lob, Portugal
185	Anderson	4.6 ± 1.6	0.2	5.0	38	56	24	−128.4	68.6	Downstream Carnwat, Canada
186	Victoria	3.2 ± 2.0	1.0	4.9	106	45	12	130.9	−15.5	Coolibah Ho, Australia
187	Roper	2.4 ± 1.5	2.7	4.8	107	47	30	134.4	−14.7	Red Rock, Australia
188	Liao	3.5 ± 2.2	3.4	4.6	274	121	42	123.5	42.2	Chiling, China
189	Orange	4.6 ± 3.5	9.2	4.6	944	851	20	17.6	−28.8	Vioolsdrift, South Africa
190	Paraquacu	4.1 ± 2.5	3.5	4.3	60	54	14	−39.0	−12.6	Pedra do Ca, Brazil
191	Contas [de]	3.4 ± 1.8	2.0	3.4	48	56	51	−39.3	−14.3	Ubaitaba, Brazil
192	Guadalquivir	3.2 ± 2.3	2.6	3.3	54	47	20	−6.0	37.5	Alcala del, Spain
193	Yaqui	2.5 ± 0.5	0.1	3.3	75	58	4	−109.5	29.2	El Novillo, Mexico
194	Colorado	2.6 ± 1.7	2.6	2.6	121	109	67	−96.1	29.3	Wharton, TX, United States
195	Rio Grande	1.5 ± 1.7	1.2	1.5	805	457	67	−97.4	25.9	Matamoros, Mexico
196	de Grey	1.4 ± 1.1	0.0	1.4	20	50	23	119.2	−20.3	Coolenar Po, Australia
197	Gascoyne	0.7 ± 0.9	0.0	0.7	90	74	41	113.8	−24.8	Nine Mile B, Australia
198	Avon	0.4 ± 0.3	0.4	0.7	166	118	30	116.1	−31.8	Wlyunga, Australia
199	Fortescue	0.3 ± 0.3	0.0	0.3	63	49	30	116.2	−21.3	Jimbegnyino, Australia
200	Murchison	0.2 ± 0.2	0.0	0.2	72	85	32	114.5	−27.9	Emu Springs, Australia
51–200 total: 3277 ± 79*			3230	3939	23 237	18 492				
1–200 total: 20 769 ± 558*			21 309	25 091	73 652	60 856				

* This number, which was estimated as the square root of the sum of the variance of the listed rivers, provides only an estimate for the true std dev of the total volume.